

Spatial-temporal patterns of inorganic nitrogen air concentrations and deposition in eastern China

Wen Xu^{1,2}, Lei Liu³, Miaomiao Cheng⁴, Yuanhong Zhao⁵, Lin Zhang⁵, Yuepeng Pan⁶,
Xiuming Zhang⁷, Baojing Gu⁸, Yi Li⁹, Xiuying Zhang³, Jianlin Shen¹⁰, Li Lu¹¹,
Xiaosheng Luo¹², Yu Zhao¹³, Zhaozhong Feng^{2*}, Jeffrey L. Collett, Jr.¹⁴, Fusuo
Zhang¹, Xuejun Liu^{1*}

¹College of Resources and Environmental Sciences, Key Laboratory of Plant-Soil Interactions of
MOE, Beijing Key Laboratory of Cropland Pollution Control and Remediation, China
Agricultural University, Beijing 100193, China

²State Key Laboratory of Urban and Regional Ecology, Research Center for Eco-Environmental
Sciences, Chinese Academy of Sciences, Shuangqing Road 18, Haidian District, Beijing, 100085,
China

³Jiangsu Provincial Key Laboratory of Geographic Information Science and Technology,
International Institute for Earth System Science, Nanjing University, Nanjing, 210023, China

⁴State Key Laboratory of Environmental Criteria and Risk Assessment, Chinese Research
Academy of Environmental Sciences, Beijing 100012, China

⁵Laboratory for Climate and Ocean-Atmosphere Sciences, Department of Atmospheric and
Oceanic Sciences, School of Physics, Peking University, Beijing 100871, China

⁶State Key Laboratory of Atmospheric Boundary Layer Physics and Atmospheric Chemistry
(LAPC), Institute of Atmospheric Physics, Chinese Academy of Sciences, Beijing, 100029, China

⁷School of Agriculture and Food, The University of Melbourne, Victoria, 3010, Australia

⁸Department of Land Management, Zhejiang University, Hangzhou 310058, People's Republic of
China

⁹Arizona Department of Environmental Quality, Phoenix, AZ 85007, USA

¹⁰Institute of Subtropical Agriculture, Chinese Academy of Sciences, Changsha 4410125, China

¹¹Institute of Surface-Earth System Science, Tianjin University, Tianjin, 300072, China

¹²Institute of Plant Nutrition, Resources and Environmental Sciences, Henan Academy of
Agricultural Sciences, Henan Key Laboratory of Agricultural Eco-environment, Zhengzhou,
450002, China

¹³State Key Laboratory of Pollution Control & Resource Reuse, School of the Environment,
Nanjing University, 163 Xianlin Ave., Nanjing, Jiangsu 210023, China

¹⁴Department of Atmospheric Science, Colorado State University, Fort Collins, Colorado, 80523
USA

*Correspondence to: X. J. Liu (liu310@cau.edu.cn) and Z.Z. Feng (fzz@rcees.ac.cn)

39

40 **Abstract:**

41 Five-year (2011-2015) measurements of gaseous NH_3 , NO_2 and HNO_3 and particulate
42 NH_4^+ and NO_3^- in air and/or precipitation were conducted at twenty-seven sites in a
43 Nationwide Nitrogen Deposition Monitoring Network (NNDMN) to better understand
44 spatial and temporal (seasonal and annual) characteristics of reactive nitrogen (N_r)
45 concentrations and deposition in eastern China. Our observations reveal annual
46 average concentrations ($16.4\text{-}32.6 \mu\text{g N m}^{-3}$), dry deposition fluxes ($15.8\text{-}31.7 \text{ kg N}$
47 $\text{ha}^{-1} \text{ yr}^{-1}$) and wet/bulk deposition fluxes ($18.4\text{-}28.0 \text{ kg N ha}^{-1} \text{ yr}^{-1}$) based on land use
48 were ranked as urban > rural > background sites. Annual concentrations and dry
49 deposition fluxes of each N_r species in air were comparable at urban and background
50 sites in northern and southern regions, but were significantly higher at northern rural
51 sites. These results, together with good agreement between spatial distributions of
52 NH_3 and NO_2 concentrations determined from ground measurements and satellite
53 observations, demonstrate that atmospheric N_r pollution is heavier in the northern
54 region than in the southern region. No significant inter-annual trends were found in
55 the annual N_r dry and wet/bulk N deposition at almost all of the selected sites. A lack
56 of significant changes in annual averages between the 2013-2015 and 2011-2012
57 periods for all land use types, suggests that any effects of current emission controls
58 are not yet apparent in N_r pollution and deposition in the region. Ambient
59 concentrations of total N_r exhibited a non-significant seasonal variation at all land use
60 types, although significant seasonal variations were found for individual N_r species
61 (e.g., NH_3 , NO_2 and $p\text{NO}_3^-$) in most cases. In contrast, dry deposition of total N_r
62 exhibited a consistent and significant seasonal variation at all land use types, with the
63 highest fluxes in summer and the lowest in winter. Based on sensitivity tests by the
64 GEOS-Chem model, we found that NH_3 emissions from fertilizer use (including
65 chemical and organic fertilizers) were the largest contributor (36%) to total inorganic
66 N_r deposition over eastern China. Our results not only improve the understanding of
67 spatial-temporal variations of N_r concentrations and deposition in this pollution
68 hotspot, but also provide useful information for policy-makers that mitigation of NH_3

69 emissions should be a priority to tackle serious N deposition in eastern China.

70 **1. Introduction**

71 In China, and globally, human activities have dramatically increased emissions
72 of nitrogen oxides ($\text{NO}_x = \text{NO} + \text{NO}_2$) and ammonia (NH_3) into the atmosphere since the
73 beginning of the industrial revolution (Galloway et al., 2008; Liu et al., 2013). NO_x
74 and NH_3 emitted to the atmosphere are transformed to nitrogen-containing particles
75 (e.g., particulate NH_4^+ and NO_3^- , and organic nitrogen) (Ianniello et al., 2010; Zhang
76 et al., 2015), which are major chemical constituents of airborne $\text{PM}_{2.5}$ (particulate
77 matter with a diameter of 2.5 μm or less) and have implications for air quality and
78 climate (Fuzzi et al., 2015). As a result of elevated reactive nitrogen (N_r) emissions,
79 nitrogen (N) deposition through dry and wet processes has also substantially increased
80 over China (Liu et al., 2013; Lu et al., 2007, 2014; Jia et al., 2014, 2016), and
81 excessive deposition of N has resulted in detrimental impacts including decreased
82 biological diversity (Bobbink et al., 2010), nutrient imbalance (Li et al., 2016),
83 increased soil acidification (Yang et al., 2015), and eutrophication of water bodies
84 (Fenn et al., 2003). Furthermore, N_r -associated haze pollution episodes, characterized
85 by high concentrations of $\text{PM}_{2.5}$, occur frequently in China, as evidenced in particular
86 in 2013 (Guo et al., 2014; Huang et al., 2014; Tian et al., 2014).

87 In order to control its notorious air pollution, China has reduced national
88 emissions of SO_2 and particulate matter by 14% and 30%, respectively, from 2005 to
89 2010 (MEPC, 2011). Additionally, stringent measures (e.g., using selective
90 catalytic/non-catalytic reduction systems, and implementing tighter vehicle emission
91 standards) were implemented during the 12th Five Year Plan (FYP) period
92 (2011-2015), with aims to reduce 2015 annual emissions of SO_2 and NO_x by 8% and
93 10%, respectively, relative to 2010 levels (Xia et al., 2016). However, there is as yet
94 no regulation or legislation that deals with national NH_3 emissions and thus emission
95 reductions of SO_2 and NO_x to achieve desired air-quality improvement goals will be
96 compromised (Gu et al., 2014). Significant increases in $\text{PM}_{2.5}$ concentrations have
97 been observed in the years 2013 and 2014 as compared to 2012, excluding the
98 influence of meteorological conditions on inter-annual variations (Liang et al., 2015).

99 Other studies with more conclusive evidence have likewise suggested that NH_3 plays
100 a vital role in sulfate formation and exacerbates severe haze pollution development in
101 urban regions of China (Wang et al., 2016), even acting as the key limiting factor for
102 the formation of secondary inorganic aerosol (Wu et al., 2016). In addition, due to
103 higher local and regional concentrations of NH_3 in the atmosphere, nitrate-driven haze
104 pollution occurred during summertime in urban environment in the North China Plain
105 (Li et al., 2018). The absolute and relative concentrations of particulate nitrate in
106 urban Beijing increased with haze development (Pan et al., 2016). Also, nitrate
107 contributed to a large fraction of the elevated $\text{PM}_{2.5}$ concentrations at a rural site in the
108 North China Plain and high NH_3 in the early morning accelerated the formation of
109 fine nitrates (Wen et al., 2015).

110 High rates of N deposition have also been observed during 2011-2014 across
111 China (Xu et al., 2015). However, to date no study, based on long-term ground-based
112 observations, has provided any information on the effectiveness of SO_2 and NO_x
113 emission controls on N deposition in China. Non-linearities have been identified
114 between reductions in emission and deposition in Europe over the last 3 decades
115 (Aguillaume et al., 2016; Fowler et al., 2007). Due to the tightly coupled yet complex
116 relationship between emissions, concentrations and deposition, long-term monitoring
117 networks can provide a test of the effectiveness of emission controls (Erisman et al.,
118 2003). Currently two national N deposition networks are operational in China, i.e. the
119 Nationwide Nitrogen Deposition Monitoring Network (NNDMN, Liu et al., 2011; Xu
120 et al., 2015) and the Chinese Ecosystem Research Network (CERS, Zhu et al., 2015).
121 The NNDMN containing 43 *in situ* monitoring sites has been operational since 2010
122 to measure wet N deposition and ambient concentrations of five major N_r species (i.e.,
123 gaseous NH_3 , NO_2 and HNO_3 , and particulate NH_4^+ and NO_3^-), the latter for
124 subsequent estimation of dry deposition. The CERS was established in 1988 and
125 mainly focused on wet N deposition at 41 field stations. In addition to ground-based
126 measurements, satellite observations enable retrieval of atmospheric NH_3 and NO_2
127 with high temporal and spatial resolutions (Dammer et al., 2016; Russell et al., 2012),
128 providing a means to reveal spatial distributions and long-term trends of ambient NH_3

129 and NO₂ levels at regional to global scales, and also to evaluate the effectiveness of
130 emission controls (Krotkov et al., 2016). However, to effectively use the vast satellite
131 data sets for environmental monitoring, it is critical to validate these remote sensing
132 observations using *in situ* surface observations (Pinder et al., 2011; Van Damme et al.,
133 2015).

134 Eastern China is a developed region with the largest densities of population,
135 economic activity and resource consumption in the country (He et al., 2015). Recent
136 satellite observations indicate that tropospheric NH₃ and NO₂ levels in eastern China
137 were both much greater than other regions of the world from 2005-2015 (Demmer et
138 al., 2016; Krotkov et al., 2016). Accordingly, this region received the highest levels of
139 dry N deposition in the world (Vet et al., 2014), and was regarded as a primary export
140 region of N deposition for neighboring countries (Ge et al., 2014). Based on
141 meta-analysis of published observations, some studies have provided information on
142 the magnitudes, spatial distributions, and decadal variations of wet/bulk N deposition
143 in China (Liu et al., 2013; Jia et al., 2014), but the analyzed data were limited to time
144 periods between 1980 and 2010. Although a recent study (Jia et al., 2016) has
145 reported a clear increasing trend of dry N deposition in eastern China between 2005
146 and 2014, considerable uncertainty may exist due to estimates of gaseous HNO₃ and
147 particulate NH₄⁺ and NO₃⁻ (*p*NH₄⁺ and *p*NO₃⁻) concentrations using NO₂ satellite data,
148 which is in part manifested by Liu et al. (2017a). Furthermore, seasonal patterns of N_r
149 concentrations and deposition have not yet been systematically investigated at a large
150 spatial scale in this region, although spatial patterns of dry N_r deposition for
151 representative months of four seasons (i.e., January for winter, April for spring, July
152 for summer, October for autumn) in 2010 have been mapped with the RAMS-CMAQ
153 model (Han et al., 2017). Thus, the spatial and temporal (annual and seasonal)
154 variations of N_r concentrations, and dry and wet deposition in eastern China require
155 further exploration using ground-based measurements, especially for time periods
156 after 2010. Our previous work (Xu et al., 2015) used multiyear measurements (mainly
157 from Jan. 2010 to Sep. 2014) at the 43 sites in the NNDMN, aiming to provide the
158 first quantitative information on atmospheric N_r concentrations and pollution status

159 across China, and to analyze overall fluxes and spatial variations of N_r deposition in
160 relation to anthropogenic N_r emissions from six regions.

161 The present study aims to examine spatial-temporal (annual and seasonal)
162 characteristics of N_r concentrations in air (NH_3 , NO_2 , HNO_3 , pNH_4^+ and pNO_3^-) and
163 precipitation (NH_4^+-N and NO_3^-N) and their corresponding dry and wet/bulk N
164 deposition, through a 5-year (2011-2015) monitoring period at 27 NNDMN sites in
165 eastern China. In addition, we compare spatial-temporal variability of measured NH_3
166 and NO_2 concentrations with variations of the corresponding satellite retrieval
167 columns, as well as inter-annual trends in N_r deposition and emissions. Finally,
168 emission sources contributing to total N deposition over eastern China are examined.

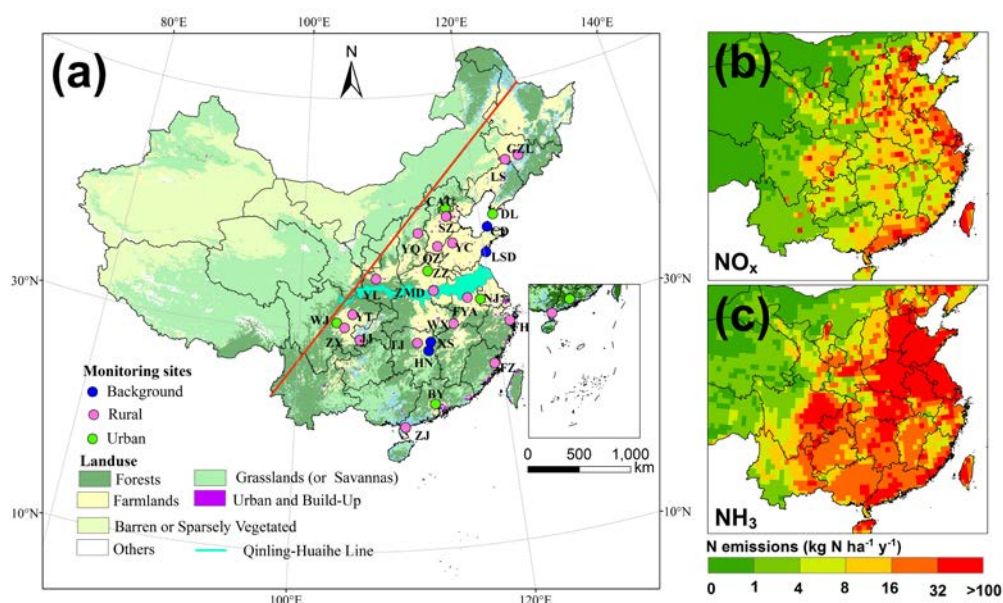
169 **2. Materials and methods**

170 **2.1 Study area and site descriptions**

171 The present study was conducted in eastern China, which is distinguished by the
172 “Hu Line” (She, 1998). This region has spatial heterogeneity in levels of economic
173 development, and significant spatial differences in NH_3 and NO_x emissions (Fig. 1b
174 and c). Thus, to better analyze spatial and temporal variabilities in measured N_r
175 concentrations and deposition, we divided eastern China into northern and southern
176 regions using the Qinling Mountains-Huaihe River line (Fig. 1a), of which the
177 division basin was based on the differences in natural conditions, agricultural
178 production, geographical features and living customs. As for specific differentiations,
179 for example, the northern region adopted a centralized domestic heating policy for
180 late autumn and winter seasons but the south has not; annual average precipitation
181 amounts were generally greater than 800 mm in the south but were less than 800 mm
182 in the north. In addition, the north is dominated by calcareous soils, which could
183 result in higher soil NH_3 volatilization (Huang et al., 2015), vs. the acidic red soil in
184 the south.

185 The NNDMN was operated in line with international standards by China
186 Agricultural University (CAU); 35 NNDMN sites were located in eastern China (Xu
187 et al., 2015). For our analysis, we considered twenty-seven sites in total, with 5-year
188 continuous data: 13 sites were located in north of the Qinling Mountains-Huaihe

189 River line (China Agricultural University-CAU, Zhengzhou-ZZ, Dalian-DL,
 190 Shuangzhuang-SZ, Quzhou-QZ, Yangqu-YQ, Zhumadian-ZMD, Yanglin-YL,
 191 Yucheng-YC, Gongzhulin-GZL, Lishu-LS, Lingshandao-LSD, Changdao-CD), and
 192 14 sites were located in south of the line (Nanjing-NJ, Baiyun-BY, Wenjiang-WJ,
 193 Wuxue-WX, Taojing-TJ, Fengyang-FY, Zhanjiang-ZJ, Fuzhou-FZ, Fenghua-FH,
 194 Ziyang-ZY, Yangting-YT, Jiangjin-JJ, Huinong-HN, Xishan-XS).



195
 196 **Figure 1.** Spatial distributions of the 27 monitoring sites (a), NO_x emissions (b)
 197 and NH_3 emissions (c) in Eastern China (NH_3 and NO_x emission data were for the
 198 year 2010 and obtained from Liu et al. (2017b)).

199 All the sites are located as far away as possible and practical from local direct
 200 emission sources to increase regional representativeness. They can be divided into
 201 three categories according to their geopolitical location and their proximity to the
 202 main emission sources: urban sites (abbreviated as U), rural sites (cropland areas, R),
 203 and background sites (coastal and forest areas, B). Information on the monitoring sites,
 204 such as land use types, coordinates, and measurement periods are listed in Table S1 of
 205 the Supplement. Detailed descriptions of all the sites including the surrounding
 206 environment and nearby emission sources can be found in Xu et al. (2015).

207 2.2 Field sampling and chemical analysis

208 Continuous measurements were performed during the period from January 2011

209 to December 2015 at the 27 study sites, except for eleven sites (ZZ, ZMD, YC, LSD,
210 NJ, WX, FYA, ZJ, YT, JJ, and HN), where field sampling was carried out after the
211 year 2011 (i.e., the years between 2012 and 2015) and/or interrupted during the period
212 due to instrument failure (details in Table S1, Supplement). Ambient N_r
213 concentrations of gaseous NH_3 and HNO_3 , and pNH_4^+ and pNO_3^- (for which the
214 empirically determined effective size cut-off for aerosol sampling is of the order of
215 $4.5 \mu m$) were measured using an active DELTA (DEnuder for Long-Term
216 Atmospheric sampling; Tang et al., 2009) system; gaseous NO_2 was sampled in three
217 replicates with passive diffusion tubes (Gradko International Limited, UK). The air
218 intakes of the DELTA system and the NO_2 tubes were mounted 2 m above the ground
219 at most sites and protected from precipitation and direct sunlight with a rigid plastic
220 box and a PVC shelter, respectively. All measurements of N_r concentration were based
221 on monthly sampling (one sample per month for each N_r species). Detailed
222 information on measuring methods and collection are given in Sect. S1 of the
223 Supplement.

224 To collect precipitation (here termed as wet/bulk deposition, which contains wet
225 and some dry deposition due to the use of an open sampler) samples, a standard
226 precipitation gauge (SDM6, Tianjin Weather Equipment Inc., China) was
227 continuously exposed beside the DELTA system (ca. 2 m). Immediately after each
228 precipitation event (08:00–08:00 next day, Greenwich Mean Time +8), samples
229 (including rain and melted snow) were collected and stored in clean polyethylene
230 bottles (50 mL) at $-18^\circ C$ until sent to the CAU laboratory for analysis. Each collector
231 was rinsed three times with high-purity water after each collection.

232 In the analytical laboratory, acid-coated denuders and aerosol filters were
233 extracted with 6 and 10 mL of high-purity water ($18.2 M\Omega$), respectively, and
234 analyzed for NH_4^+-N with an AA3 continuous-flow analyzer (CFA) (BranC Luebbe
235 GmbH, Norderstedt, Germany). Carbonate-coated denuders and filters were both
236 extracted with 10 mL 0.05% H_2O_2 solution followed by analysis of NO_3-N using the
237 same CFA. NO_2 samples, extracted with a solution containing sulfanilamide, H_3PO_4 ,
238 and N-1-naphthylethylene-diamine, were determined using a colorimetric method by

239 absorption at a wavelength of 542 nm (Xu et al., 2016). Precipitation samples were
240 filtered through a syringe filter (0.45 μ m, Tengda Inc., Tianjin, China) and analyzed
241 for NH_4^+ -N and NO_3^- -N using the CFA as mentioned above. Quality assurance and
242 quality control procedures adopted in the analytical laboratory are described by Xu et
243 al. (2017). Further details of precipitation measurement, samples handling, and
244 chemical analysis are reported in Xu et al. (2015).

245 **2.3 Deposition estimate**

246 Wet/bulk deposition of NH_4^+ -N and NO_3^- -N were calculated per month and year
247 by multiplying the precipitation amount by their respective volume-weighted mean
248 (VWM) concentrations. The dry deposition flux of gaseous and particulate N_r species
249 was calculated as the product of measured concentrations by modeled deposition
250 velocities (V_d). The dry deposition velocities of five N_r species were calculated by the
251 GEOS (Goddard Earth Observing System)-Chem chemical transport model (CTM)
252 (Bey et al., 2001; <http://geos-chem.org>), and have been reported in a companion paper
253 (Xu et al., 2015). In brief, the model calculation of dry deposition of N_r species
254 follows a standard big-leaf resistance-in-series model as described by Wesely (1989)
255 for gases and Zhang et al. (2001) for aerosol. We used archived hourly V_d from
256 January 2011 to May 2013 and filled the gap for the period (from June 2013 to
257 December 2015) when GEOS meteorological data are unavailable using the mean
258 values calculated from all the available simulations. The monthly V_d at each site was
259 averaged from the hourly dataset.

260 **2.4 Satellite retrievals of NH_3 and NO_2**

261 Comparisons between satellite observations and ground-based measurements
262 were evaluated at the twenty-seven sites in order to accurately examine the
263 spatial-temporal pattern of NH_3 and NO_2 concentrations. For NH_3 , we used the
264 products retrieved from the Infrared Atmospheric Sounding Interferometer (IASI)
265 instrument (aboard the MetOp-A platform), which crosses the equator at a mean local
266 solar time of 9:30 a.m. and 9:30 p.m. The IASI- NH_3 product is based on the
267 calculation of a spectral hyperspectral range index and subsequent conversion to NH_3
268 total columns via a neural network. The details of the IASI- NH_3 retrieval method are

269 described in Whitburn et al. (2016). We only considered the observations from the
270 morning overpass as they are generally more sensitive to NH₃ because of higher
271 thermal contrast at this time of day (Van Damme et al., 2015; Dammers et al., 2016).
272 The daily IASI-NH₃ data (provided by the Atmospheric Spectroscopy Group at
273 Université Libre De Bruxelles, data available at <http://iasi.aeris-data.fr/NH3/>) from 1
274 January 2011 to 31 December 2015 was used for the spatial analysis in the present
275 study. For the temporal analysis, we used the IASI_NH₃ from 1 January 2011 to 30
276 September 2014 because an update of the input meteorological data on 30 September
277 2014 had caused a substantial increase in the retrieved atmospheric NH₃ columns.
278 Only observations with a cloud coverage lower than 25%, and relative error lower
279 than 100% or absolute error smaller than 5×10^{15} molecules cm⁻² were processed. The
280 methodology is provided in detail in Liu et al. (2017b). In brief, all observations were
281 gridded to a 0.5° latitude × 0.5° longitude grid, and then we calculated the monthly
282 arithmetic mean by averaging the daily values with observations points within each
283 grid cell. Similarly, we calculated the annual arithmetic mean by averaging the daily
284 values with observations points within the grid cell over the whole year.

285 For NO₂ we used the products from the Ozone Monitoring Instrument (OMI)
286 resided on NASA's EOS-Aura satellite, which was launched in July 2004 into a
287 sun-synchronous orbit with a local equator crossing time at approximately 1:45 p.m.
288 OMI detects the backscattered solar radiation from the Earth's atmosphere within the
289 UV-vis spectral window between 270-500 nm, to achieve nearly global coverage daily,
290 with a spatial resolution ranging from 13 km × 24 km at nadir to 24 km × 128 km at
291 the edge of the swath (Russell et al., 2012). We used tropospheric NO₂ retrievals from
292 the DOMINO (Dutch Finnish Ozone Monitoring Instrument) algorithm version 2. The
293 retrieval algorithm is described in detail in Boersma et al. (2007). The tropospheric
294 NO₂ columns used in this study are monthly means from 1 January 2011 to 30
295 December 2015 with a spatial resolution of 0.125° latitude × 0.125° longitude (data
296 available at <http://www.temis.nl/airpollution/no2.html>).

297 **2.5 Statistical analysis**

298 One-way analysis of variance (ANOVA) and two-independent-samples *t* tests

299 were applied to detect significant differences in seasonal mean concentrations and
300 deposition fluxes of measured N_r species as well as their annual mean deposition
301 fluxes for three land use types (rural, urban and background). As there was large
302 site-to-site variability in annual N_r concentrations and deposition fluxes at monitoring
303 sites within the same land use types, averaging data into annual values for land use
304 types is unlikely to be truly representative of actual trends. Thus, annual trends of the
305 variables were evaluated at a single site scale rather than by land use type. Trend
306 analysis was conducted using Theil regression (Theil, 1992) and the Mann-Kendall
307 test (Gilbert, 1987; Marchetto et al., 2013). We defined an increasing (decreasing)
308 trend as a positive (negative) slope of the Theil regression, while a statistical
309 significance level ($p < 0.01$) of a trend was evaluated by the non-parametric
310 Mann-Kendall test (p value). Non-parametric methods usually have the advantage of
311 being insensitive to outliers, and allow missing data and non-normal distribution of
312 data (Gilbert, 1987; Salmi et al., 2002), appropriate for the analyzed data set. The
313 Mann-Kendall method is appropriate for detection of monotonic trends in data series
314 that have no seasonal variation or autocorrelation. Atmospheric concentrations and
315 deposition fluxes of N_r species, however, generally have distinct seasonal variability
316 (Pan et al., 2012) and the Mann-Kendall test is thus applied to annual values.

317 Satellite observations during 2005-2015 indicate that tropospheric NO_2 levels
318 peaked in 2011 over China (Krotkov et al., 2016; Duncan et al., 2016) and NO_x
319 emissions peaked in 2011/2012 (Miyazaki et al., 2017; van der A et al., 2017; Souri et
320 al., 2017). To assess the impact of emission control measures on measured N_r
321 concentrations and deposition fluxes at different land use types, we compared
322 arithmetic mean values averaged from the last 3-year period (2013-2015) with those
323 averaged from the first 2-year period (2011-2012) for monitoring sites with
324 continuous 5-year measurements (twenty-one sites for dry, and seventeen sites for
325 wet/bulk). Seasonal concentrations and deposition fluxes of measured N_r species were
326 calculated using the arithmetic average of matched seasons during the sampling
327 periods; spring refers to March-May, summer covers June-August, autumn refers to
328 September-November, and winter covers December-February.

329

330 **3. Results**331 **3.1 Spatial variability in concentrations of N_r species in air and precipitation**

332 Summary statistics of monthly mean concentrations of NH₃, NO₂, HNO₃, pNH₄⁺,
 333 and pNO₃⁻ at the twenty-seven monitoring sites during 2011-2015 are listed in Table
 334 S2 of the Supplement. Monthly mean concentrations of NH₃, NO₂, HNO₃, pNH₄⁺, and
 335 pNO₃⁻ ranged from 0.16 (TJ)-39.57 (WJ), 0.55 (LS)-29.06 (WJ), 0.04 (YQ)-4.93
 336 (CAU), 0.11 (ZY)-57.20 (QZ), and 0.01 (DL)-32.06 (ZZ) µg N m⁻³, respectively. On
 337 the basis of geographical location and classification of each site, the annual mean
 338 concentrations of each N_r species were calculated for three land use types in eastern
 339 China and its northern and southern regions (Table 1).

340 **Table 1.** Annual average (standard error) concentrations of various N_r compounds in
 341 air and precipitation at different land use types in eastern China and its northern and
 342 southern regions for the 5-year period 2011-2015.

Region ^a	LUT ^b	Ambient conc. µg N m ⁻³						Rainwater conc. mg N L ⁻¹		
		NH ₃	NO ₂	HNO ₃	pNH ₄ ⁺	pNO ₃ ⁻	Total N _r	NH ₄ ⁺	NO ₃ ⁻	TIN
EC	Urban	8.5	10.2	1.6	8.2	4.0	32.6	1.6	1.9	3.5
	(n=6)	(1.4)	(1.0)	(0.2)	(1.8)	(0.8)	(4.1)	(0.3)	(0.2)	(0.5)
	Rural	7.2	6.0	1.2	6.7	2.8	23.9	1.7	1.4	3.1
	(n=17)	(0.9)	(0.5)	(0.1)	(1.1)	(0.3)	(2.7)	(0.2)	(0.2)	(0.4)
BKD ^c		3.9	5.2	0.9	4.5	1.9	16.4	1.4	1.2	2.6
	(n=4)	(0.6)	(0.3)	(0.1)	(0.4)	(0.3)	(1.4)	(0.3)	(0.4)	(0.6)
NREC	Urban	8.1	11.7	1.6	8.6	5.1	35.1	2.2	2.4	4.6
	(n=3)	(2.4)	(1.6)	(0.3)	(2.3)	(1.4)	(7.7)	(0.4)	(0.2)	(0.4)
	Rural	9.9	7.4	1.4	9.2	3.7	31.6	2.4	2.0	4.4
	(n=8)	(1.2)**	(0.7)*	(0.1)*	(1.9)*	(0.5)*	(3.8)**	(0.3)**	(0.2)**	(0.4)**
BKD		4.7	5.7	1.0	5.1	2.4	18.8	1.8	1.5	3.3
	(n=2)	(0.6)	(0.3)	(0.1)	(0.2)	(0.3)	(0.1)	(0.2)	(0.3)	(0.1)
SREC	Urban	8.9	8.7	1.6	7.9	2.9	30.1	1.1	1.5	2.6
	(n=3)	(1.8)	(0.6)	(0.1)	(3.1)	(0.2)	(4.5)	(0.3)	(0.3)	(0.6)
	Rural	4.9	4.6	1.0	4.5	1.9	17.0	1.1	0.9	2.0
	(n=9)	(0.6)	(0.6)	(0.1)	(0.6)	(0.2)	(1.7)	(0.2)	(0.1)	(0.3)
BKD		3.1	4.7	0.8	4.0	1.4	14.0	1.0	0.6	1.6
	(n=2)	(0.7)	(0.4)	(0.1)	(0.2)	(0.2)	(0.6)	(0.0)	(0.0)	(0.0)

343 ^aEC: eastern China; NREC: northern region of eastern China; SREC: southern region
344 of eastern China. ^bLUT: land use type; n denotes number of monitoring sites. ^cBKD:
345 Background. * and ** denote significance at the 0.05 and 0.01 probability levels for
346 difference in annual mean N_r concentrations at a given site type between northern and
347 southern regions, respectively.

348 In eastern China, annual mean concentrations of NH₃, NO₂, HNO₃, pNH₄⁺, and
349 pNO₃⁻ at the urban sites (averages for the 5-year, 1.6 ± 0.2 (for HNO₃) to 10.2 ± 1.0
350 (for NO₂) µg N m⁻³) increased by 18, 70, 33, 23, and 43%, respectively, compared
351 with their corresponding concentrations at the rural sites (1.2 ± 1.0 (for HNO₃) to 7.2
352 ± 0.9 (for NH₃) µg N m⁻³); they also increased by 78-118% compared with the
353 concentrations at the background sites (0.9 ± 0.1 (for HNO₃) to 5.2 ± 0.3 (for NO₂) µg
354 N m⁻³) (Table 1). Analogous patterns also occurred for all measured N_r in each region,
355 except for NH₃ and pNH₄⁺ in the northern region, for which the mean concentrations
356 were 18% and 7% lower at the urban sites than at the rural sites, respectively.

357 Comparing northern vs. southern regions (Table 1), at urban sites the annual
358 mean concentrations of NH₃, HNO₃, and pNH₄⁺ showed smaller non-significant
359 differences (-1~9%), whereas NO₂ and pNO₃⁻ showed larger non-significant increases
360 (34 and 76%, respectively) in the north. By contrast, the mean concentrations of all
361 measured N_r species were significantly (*p*<0.05) higher (by 40-104%) at rural sites in
362 northern region. Similarly, individual concentrations at background sites were 21-71%
363 higher in the northern than southern region. Averaged across three land use types, the
364 annual mean N_r concentrations of five N_r species in the north increased to varying
365 extent (by 84% for pNO₃⁻, 63% for pNH₄⁺, 57% for NH₃, 47% for NO₂, and 28% for
366 HNO₃) compared with those in the south. The annual concentrations of total N_r (i.e.,
367 the sum of five N_r species) decreased in the order urban > rural > background in
368 eastern China as a whole and in the north and south regions; further, the annual total
369 N_r concentrations at urban and background sites were 17 and 34% higher (*p*>0.05) in
370 the north than in the south, respectively, whereas those at northern rural sites (31.6 ±
371 3.8 µg N m⁻³) were significantly (*p*<0.05) higher than the means at southern rural sites
372 (17.0 ± 1.7 µg N m⁻³).

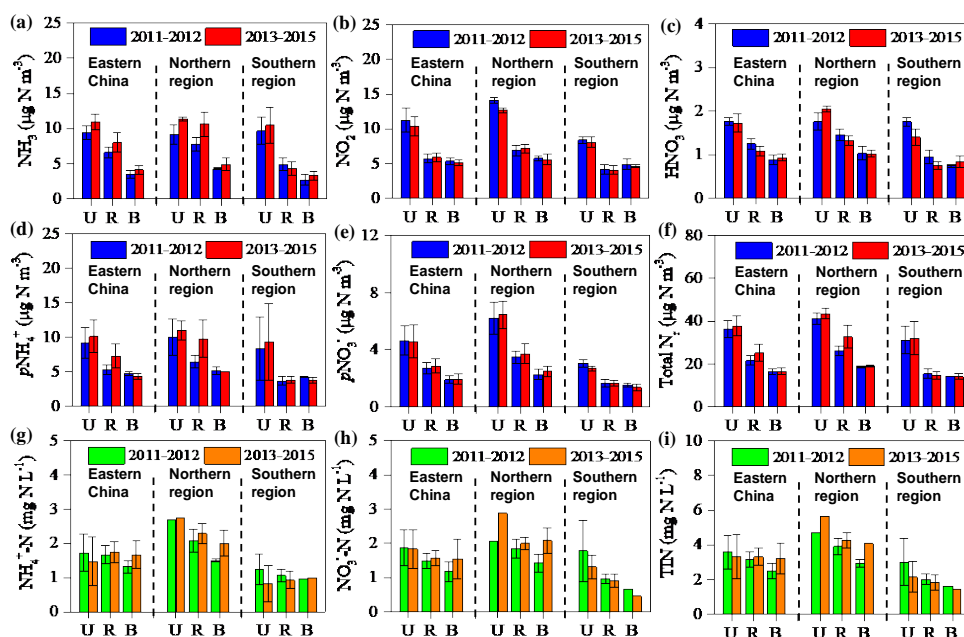
373 The monthly VWM concentrations of $\text{NH}_4^+\text{-N}$, $\text{NO}_3^-\text{-N}$, and TIN (the sum of
374 $\text{NH}_4^+\text{-N}$ and $\text{NO}_3^-\text{-N}$) were in the ranges 0.01 (BY)-26.77 (YC), 0.06 (XS)-28.92 (WJ),
375 and 0.09 (XS)-50.29 (YC) mg N L^{-1} , respectively (Table S3, Supplement). In eastern
376 China and in each region, the annual VWM concentrations of $\text{NO}_3^-\text{-N}$ and TIN
377 showed a declining trend of urban > rural > background, whereas those of $\text{NH}_4^+\text{-N}$
378 followed the order rural \geq urban > background (Table 1). Comparing northern and
379 southern regions, the annual concentrations of $\text{NH}_4^+\text{-N}$, $\text{NO}_3^-\text{-N}$, and TIN were
380 comparable at urban and background sites, and were significantly ($p < 0.05$) higher at
381 northern rural sites.

382 **3.2 Annual variability in concentrations of N_r species in air and precipitation**

383 During the 2011-2015 period the annual mean concentrations of measured N_r
384 species in air exhibited no significant trends at the twenty-one selected sites except for
385 NH_3 at four sites (ZZ, DL, ZMD, YL), HNO_3 at three sites (DL, LSD, BY), $p\text{NH}_4^+$
386 at one site (XS), and total N_r at three sites (ZMD, YL, WJ) (Fig. S1a-f, Supplement).
387 Similarly, no significant trends were found for the annual VWM concentrations of
388 $\text{NH}_4^+\text{-N}$, $\text{NO}_3^-\text{-N}$, and TIN in precipitation at the seventeen selected sites, with the
389 exception of $\text{NO}_3^-\text{-N}$ at one site (SZ) (Fig. S2a-c, Supplement).

390 Fig. 2 compares annual average concentrations of all measured N_r species
391 between the periods 2013-2015 and 2011-2012 for three land use types. In eastern
392 China the mean concentrations of NH_3 and $p\text{NH}_4^+$ showed non-significant increases
393 (10-38%) at all land use types except $p\text{NH}_4^+$ at background sites, which showed a
394 small reduction (8%) (Fig. 2a, d). By contrast, the mean concentrations of remaining
395 N_r species at three land use types showed smaller and non-significant changes: -8~3%
396 for NO_2 (Fig. 2b), -13~5% for HNO_3 (Fig. 2c), and -1~5% for $p\text{NO}_3^-$ (Fig. 2e). The
397 relative changes in the annual total N_r concentration were also not significant, with the
398 largest increase at rural sites (16%) and smaller increases at urban (4%) and
399 background (1%) sites (Fig. 2f). Separated by regions, annual mean concentrations of
400 five N_r species at three land use types mostly showed increases (4-57%) in the north,
401 and reductions (0.3-21%) in the south (Fig. 2a-f). The relative changes in individual
402 concentrations at northern rural sites (9% reduction for HNO_3 , and 9-52% increases

403 for the other species) and southern rural sites (4% increase for $p\text{NH}_4^+$, and 0.3-21%
 404 reductions for other species) were not significant. The annual total N_r concentrations
 405 showed small relative changes (from -1% to 5%) across all land use types in the two
 406 regions, except at northern rural sites, which exhibited a larger but non-significant
 407 increase (25%) (Fig. 2f). Due to significant interannual variability, longer records are
 408 needed to better assess the significance of any concentration changes.



409
 410 **Figure 2.** Comparison of annual mean concentrations of (a) NH_3 ; (b) NO_2 ; (c) HNO_3 ;
 411 (d) $p\text{NH}_4^+$; (e) $p\text{NO}_3^-$; and (f) total N_r : sum of all measured N_r in air and
 412 volume-weighted concentrations of NH_4^+ (g); NO_3^- (h) and total inorganic N (TIN):
 413 sum of NH_4^+ and NO_3^- (i) in precipitation between the 2011-2012 period and the
 414 2013-2015 period for different land use types in eastern China and its northern and
 415 southern regions. U, R, and B denote urban, rural, and background sites, respectively.
 416 The number of sites for each land use type in each region can be found in Table S1 in
 417 the Supplement. The error bars are the standard errors of means.

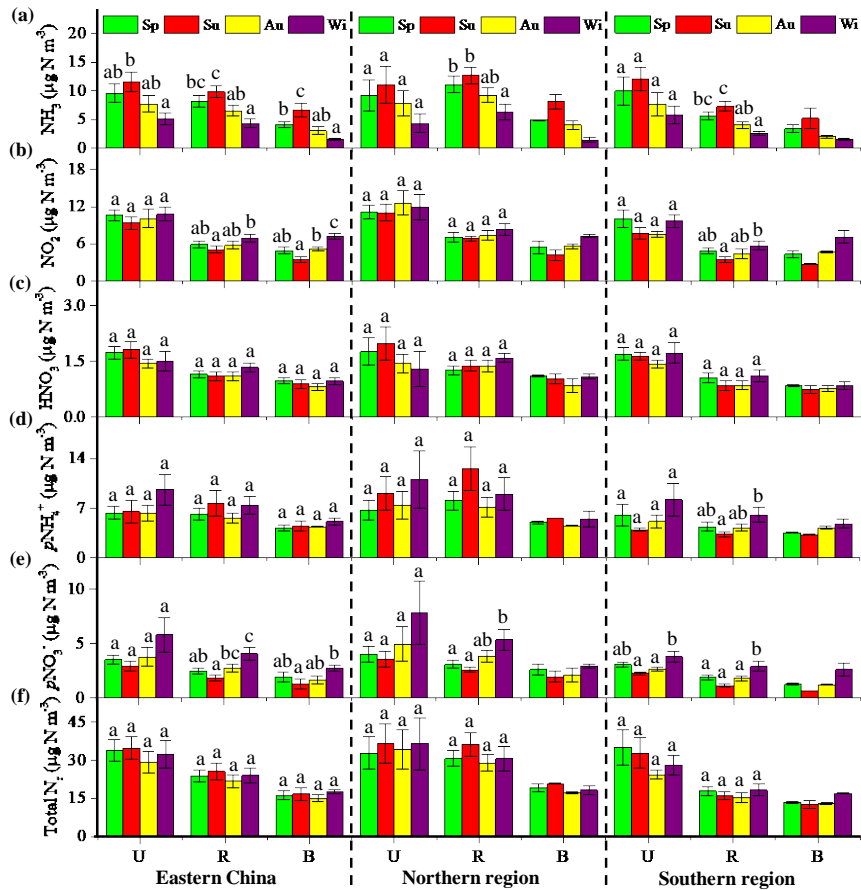
418
 419 In eastern China, the annual VWM concentrations of $\text{NH}_4^+\text{-N}$, $\text{NO}_3^-\text{-N}$ and TIN
 420 showed the largest increase of 26-31% at background sites, a smaller increase of 4-5%
 421 at rural sites, and a decrease of 2-14% at urban sites; however, those changes were not
 422 significant (Fig. 2g-i). Regionally, their respective concentrations showed increases

423 (3-45%) in the north and reductions (5-33%) in the south, except for a small increase
424 (4%) in $\text{NH}_4^+\text{-N}$ at background sites.

425 **3.3 Seasonal variability in concentrations of N_r species in air and precipitation**

426 Fig. 3 shows seasonal patterns of NH_3 , NO_2 , HNO_3 , $p\text{NH}_4^+$, $p\text{NO}_3^-$ and total N_r
427 concentrations for three land use types in eastern China and its northern and southern
428 regions, averaged from corresponding measurements at the twenty-seven study sites
429 (details for each site are given in Tables S4-S9 of the Supplement). Average NH_3
430 concentrations at all land use types decreased in the order summer > spring > autumn >
431 winter, and significant seasonal differences generally occurred between summer and
432 winter (Fig. 3a). Conversely, the average NO_2 concentration generally showed the
433 highest value in winter and the lowest in summer; differences between seasonal
434 concentrations were sometimes significant at rural sites in the south and background
435 sites, but not at urban sites (Fig. 3b). The seasonal changes in the HNO_3 concentration
436 were generally small and not significant for all land use types (Fig. 3c).

437 The average $p\text{NH}_4^+$ concentration exhibited a non-significant seasonal variation
438 across all land use types, except for southern rural sites which showed significantly
439 higher values in winter than in summer (Fig. 3d). The highest $p\text{NH}_4^+$ concentrations
440 mostly occurred in winter. The average $p\text{NO}_3^-$ concentrations at all land use types
441 followed the order winter > spring, ~ autumn > summer; the seasonal changes are
442 sometimes significant, except for urban sites in eastern China and its northern region
443 (Fig. 3e). The average concentration of total N_r usually showed small and
444 non-significant seasonal differences for all land use types (Fig. 3f).



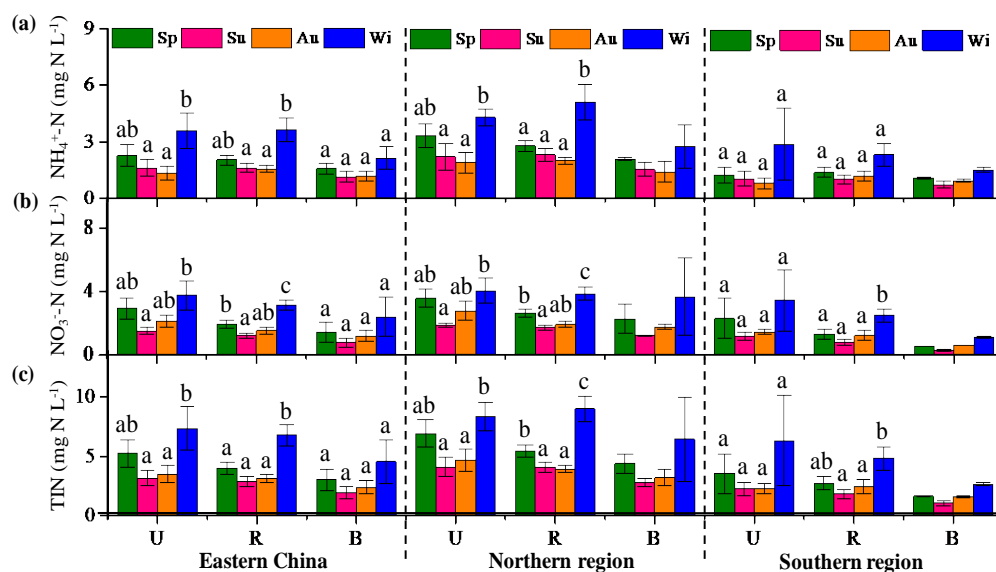
445

446 **Figure 3.** Seasonal mean concentrations averaged over 2011-2015 of (a) NH_3 ; (b)
 447 NO_2 ; (c) HNO_3 ; (d) $p\text{NH}_4^+$; (e) $p\text{NO}_3^-$; and (f) total N_r : sum of all measured N_r in air
 448 at different land use types in eastern China and its northern and southern regions. Sp,
 449 Su, Au, and Wi represent spring, summer, autumn, and winter, respectively. U, R, and
 450 B denote urban, rural, and background sites, respectively. The number of sites for
 451 each land use type in each region can be found in Table 1. The error bars are the
 452 standard errors of means, and values without same letters on the bars denote
 453 significant differences between the seasons ($p < 0.05$).

454

455 In eastern China and its two regions, the seasonal VWM concentrations of
 456 $\text{NH}_4^+\text{-N}$, $\text{NO}_3^-\text{-N}$ and TIN in precipitation at three land use types (averaged from the
 457 twenty-seven sites, details in Tables S10-S12 of the Supplement) showed a similar
 458 seasonal pattern, with the highest values in winter and the lowest in summer or
 459 autumn (Fig. 4a-c). Significant seasonal differences usually occurred between winter
 460 and the other three seasons at all land use types, except background sites and southern

461 urban sites.



462

463 **Figure 4.** Seasonal mean concentrations averaged over 2011-2015 of NH_4^+ (a); NO_3^-
 464 (b) and total inorganic N (TIN): sum of NH_4^+ and NO_3^- (c) in precipitation at different
 465 land use types in eastern China and its northern and southern regions. Sp, Su, Au, and
 466 Wi represent spring, summer, autumn, and winter, respectively. U, R, and B denote
 467 urban, rural, and background sites, respectively. The number of sites for each land use
 468 type in each region can be found in Table 1. The error bars are the standard errors of
 469 means, and values without same letters on the bars denote significant differences
 470 between the seasons ($p < 0.05$).

471 3.4 Spatial variability in dry and wet/bulk N deposition of N_r species

472 Dry deposition fluxes of NH_3 , HNO_3 , NO_2 , $p\text{NH}_4^+$, and $p\text{NO}_3^-$ ranked in the
 473 order urban > rural > background in eastern China and in both southern and northern
 474 regions (except for $p\text{NH}_4^+$ in the north) (Table 2). Comparing northern and southern
 475 regions, at urban sites the mean dry $p\text{NH}_4^+$ deposition was slightly higher (2%) in the
 476 north, whereas larger enhancements (24-69%) in the mean fluxes were found in the
 477 north for the remaining N_r species. By contrast, individual fluxes were significantly
 478 higher (by 64-138%) at northern rural sites, except for HNO_3 which showed a large
 479 non-significant increase (58%). At northern background sites, the mean dry deposition
 480 fluxes of NH_3 and NO_2 were much higher (159%) and lower (68%), respectively;
 481 however, only small differences in the means were found for HNO_3 (6% lower in the

482 north), $p\text{NH}_4^+$ (5% lower), and $p\text{NO}_3^-$ (14% higher). The spatial pattern of total N dry
 483 deposition flux (the sum of the fluxes of the five N_r species) by land use types ranked
 484 in the same order as individual N_r species in eastern China. Compared with the
 485 southern region, mean total N fluxes in the north region were significantly higher (by
 486 85%) at rural sites, but showed non-significant increases at urban and background
 487 sites (33 and 38%, respectively).

488 The wet/bulk deposition fluxes of $\text{NH}_4^+\text{-N}$, $\text{NO}_3^-\text{-N}$, and TIN ranked in the order
 489 urban > rural > background in eastern China and in each region (except for $\text{NH}_4^+\text{-N}$ in
 490 the south) (Table 2). In addition, their respective fluxes were generally comparable in
 491 northern and southern regions.

492

493 **Table 2.** Annual average (standard error) dry and wet/bulk deposition fluxes (kg N
 494 $\text{ha}^{-1} \text{yr}^{-1}$) of various N_r compounds at different land use types in eastern China and its
 495 northern and southern regions for the 5-year period 2011-2015.

Region ^a	LUT ^b	Dry deposition					Wet/bulk deposition			
		NH_3	NO_2	HNO_3	$p\text{NH}_4^+$	$p\text{NO}_3^-$	Total N_r	NH_4^+	NO_3^-	TIN
EC	Urban	12.6	4.4	7.7	4.8	2.1	31.7	12.6	15.4	28.0
	(n=6)	(1.4)	(1.2)	(1.6)	(1.4)	(0.5)	(4.6)	(1.9)	(0.7)	(2.2)
	Rural	9.1	2.9	4.6	4.0	1.5	22.1	11.9	10.2	22.1
	(n=17)	(0.9)	(0.3)	(0.6)	(0.7)	(0.2)	(2.3)	(1.0)	(0.5)	(1.4)
	BKD ^c	7.9	1.8	3.5	1.9	0.8	15.8	10.7	7.7	18.4
	(n=4)	(2.1)	(0.6)	(0.2)	(0.3)	(0.1)	(1.5)	(1.8)	(0.3)	(1.8)
NREC	Urban	13.9	5.2	9.4	4.9	2.7	36.2	13.9	14.1	28.0
	(n=3)	(1.9)	(2.5)	(3.0)	(1.9)	(1.0)	(8.2)	(3.5)	(1.0)	(4.4)
	Rural	12.1 ^{**}	3.6 [*]	5.7	5.7 [*]	2.1 ^{**}	29.3 ^{**}	12.3	10.3	22.6
	(n=8)	(1.3)	(0.4)	(1.0)	(1.2)	(0.3)	(3.2)	(1.3)	(0.7)	(1.8)
	BKD	11.4	0.9	3.4	1.9	0.8	18.4	7.8	7.6	15.4
	(n=2)	(0.6)	(0.7)	(0.3)	(0.7)	(0.2)	(0.7)	(1.4)	(0.8)	(0.6)
SREC	Urban	11.2	3.6	5.9	4.8	1.6	27.2	11.4	16.6	28.0
	(n=3)	(2.0)	(0.3)	(0.6)	(2.6)	(0.2)	(4.0)	(2.0)	(0.4)	(2.1)
	Rural	6.5	2.2	3.6	2.4	1.0	15.8	11.6	10.2	21.8
	(n=9)	(0.5)	(0.4)	(0.6)	(0.4)	(0.2)	(1.4)	(1.5)	(0.9)	(2.2)
	BKD	4.4	2.7	3.6	2.0	0.7	13.3	13.6	7.9	21.5
	(n=2)	(1.0)	(0.2)	(0.3)	(0.1)	(0.1)	(0.7)	(0.1)	(0.1)	(0.1)

496 ^a EC: eastern China; NREC: northern region of eastern China; SREC: southern region

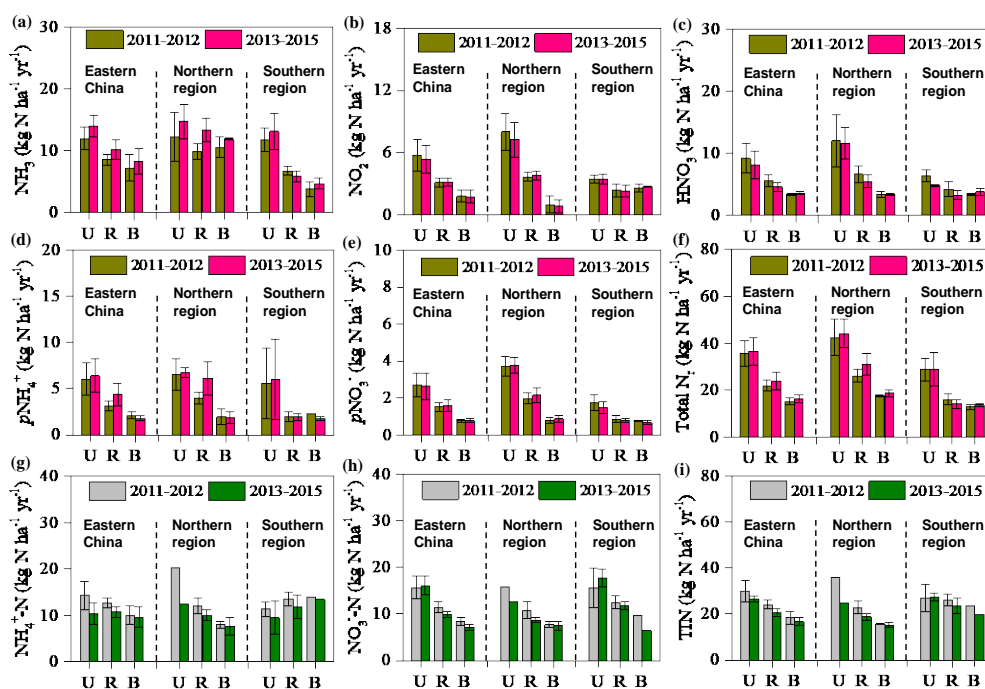
497 of eastern China. ^b LUT: land use type; n denotes number of monitoring sites. ^c BKD:
498 Background. * and ** denote significance at the 0.05 and 0.01 probability levels for
499 difference in annual mean N_r concentrations at a given site type between northern and
500 southern regions, respectively.

501 **3.5 Annual variability in dry and wet/bulk N deposition**

502 The annual trends of dry deposition fluxes of individual N_r species at the
503 twenty-one selected sites are consistent with trends in their respective ambient
504 concentrations, except for HNO_3 at three sites (SZ, LSD, and ZY) (Figs. S3a-e and
505 S1a-e, Supplement). A consistent picture is also seen for the total dry N deposition
506 fluxes at all but two sites (DL and WJ) (Figs. S3f and S1f, Supplement). Similarly, the
507 annual trends of wet/bulk deposition fluxes of NH_4^+ -N, NO_3^- -N and TIN at seventeen
508 selected sites are similar to their respective concentrations in precipitation (Fig. S4a-c,
509 Supplement).

510 In eastern China the annual average dry deposition fluxes of NH_3 , NO_2 , HNO_3 ,
511 pNH_4^+ and pNO_3^- showed non-significant increases (2-39%) or reductions (1-19%)
512 between the periods 2011-2012 and 2013-2015 at the three land use types (Fig. 5a-e),
513 similar in sign and magnitude to their respective concentrations described earlier. The
514 annual average total N dry deposition fluxes showed small and non-significant
515 increases across the study periods: 2% at urban sites, 9% at rural sites, and 7% at
516 background sites (Fig. 5f). The sign and magnitude of period-to-period changes in dry
517 deposition and ambient concentrations of all measured N_r species were generally
518 similar between the southern and northern regions.

519 Wet/bulk deposition fluxes of NH_4^+ -N, NO_3^- -N, and TIN generally decreased
520 (4-29%) between 2011-2012 and 2013-2015 periods at all land use types in eastern
521 China; one exception was NO_3^- -N, which exhibited a small increase (3%) at urban
522 sites (Fig. 5g-i). Similar tendencies were also observed in both northern and southern
523 regions.



524

525 **Figure 5.** Comparison of dry deposition of (a) NH_3 ; (b) NO_2 ; (c) HNO_3 ; (d) $p\text{NH}_4^+$;

526 (e) $p\text{NO}_3^-$; and (f) total N_r : sum of all measured N_r in air and wet/bulk deposition of

527 NH_4^+ (g); NO_3^- (h) and total inorganic N (TIN): sum of NH_4^+ and NO_3^- (i) in

528 precipitation between the 2011-2012 period and the 2013-2015 period for different

529 land use types in eastern China and its northern and southern regions. U, R, and B

530 denote urban, rural, and background sites, respectively. The number of sites for each

531 land use type in each region can be found in Table S1 in the Supplement. The error

532 bars are the standard errors of means.

533

534 3.6 Seasonal variability in dry and wet/bulk deposition of N_r species

535 Seasonal variations of dry deposition of individual N_r species at each site are

536 shown in Tables S4-S9 in the Supplement. In eastern China and in each region, dry

537 NH_3 deposition fluxes at all land use types followed the order summer > spring >

538 autumn > winter, with the seasonal changes usually significantly different (Fig. 6a).

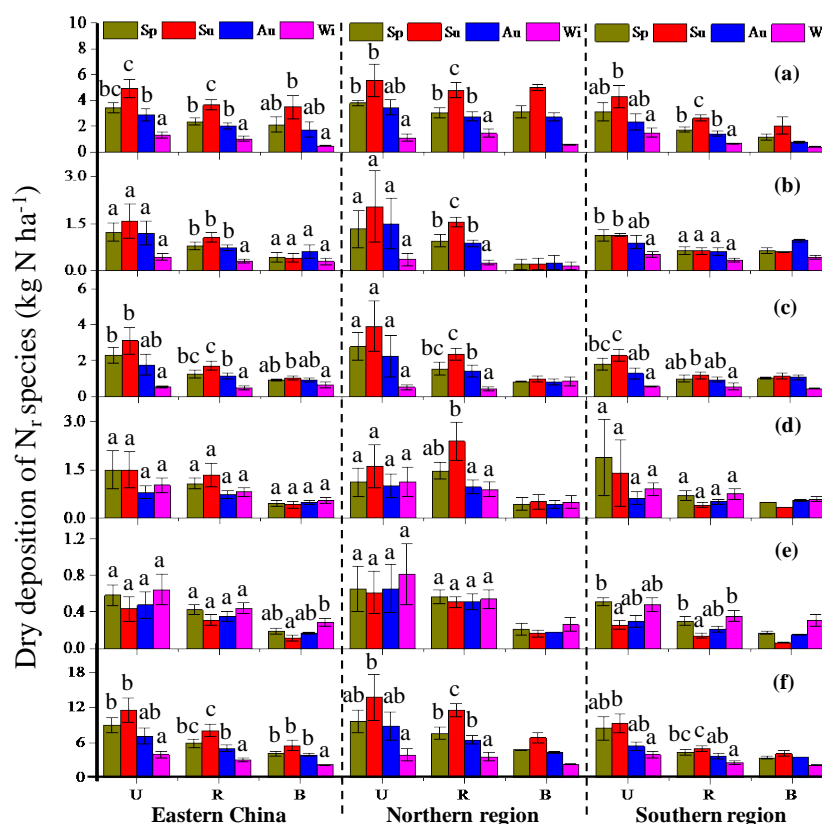
539 Similarly, dry the NO_2 deposition flux was also at its minimum in winter, but its

540 maximum was found in summer at urban and rural sites and in autumn at background

541 site; seasonal differences in most cases were not significant (Fig. 6b). Seasonal

542 patterns of dry HNO_3 deposition flux at all land use types were similar to those for dry

543 NH₃ deposition fluxes, and the resulting seasonal changes were sometimes significant,
 544 except at northern urban sites (Fig. 6c).



545

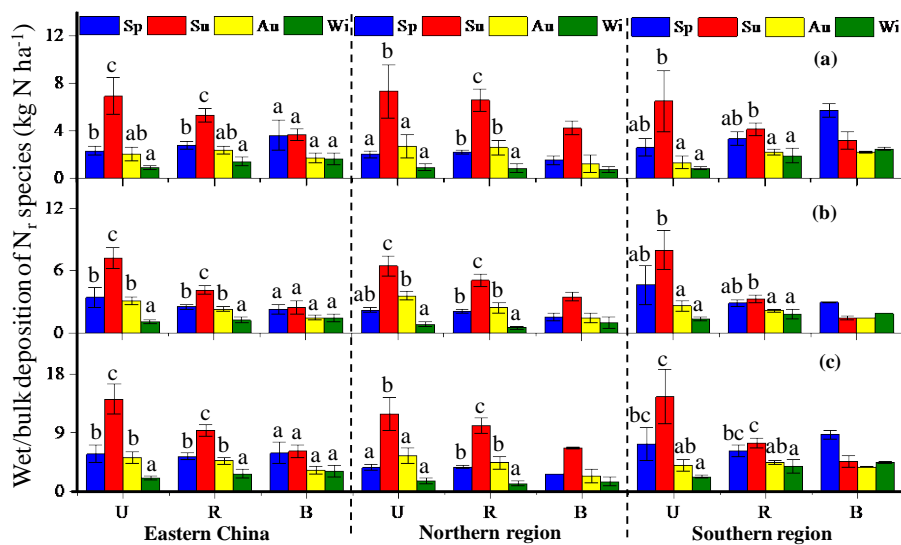
546 **Figure 6.** Seasonal mean dry deposition averaged over 2011-2015 of (a) NH₃; (b)
 547 NO₂; (c) HNO₃; (d) *p*NH₄⁺; (e) *p*NO₃⁻; and (f) total N_r: sum of all measured N_r in air
 548 at different land use types in eastern China and its northern and southern regions. Sp,
 549 Su, Au, and Wi represent spring, summer, autumn, and winter, respectively. U, R, and
 550 B denote urban, rural, and background sites, respectively. The number of sites for
 551 each land use type in each region can be found in Table 2. The error bars are the
 552 standard errors of means, and values without same letters on the bars denote
 553 significant differences between the seasons (*p*<0.05).

554

555 Dry *p*NH₄⁺ deposition fluxes peaked in spring or summer at urban and rural sites,
 556 but remained at similar levels across the four seasons at background sites; however,
 557 no significant seasonal variations were found at any land use types except for rural
 558 sites in the north (Fig. 6d). Dry *p*NO₃⁻ deposition fluxes were higher in spring and
 559 winter than in summer and autumn at all land use types, and the seasonal changes

560 were sometimes significant at background sites and at southern urban and rural sites
 561 (Fig. 6e). Total dry N deposition fluxes at all land use types showed similar seasonal
 562 variations to dry NH₃ deposition, with the highest values in summer and the lowest in
 563 winter; significant seasonal differences generally were observed between winter and
 564 the other three seasons (Fig. 6f).

565 Wet/bulk deposition fluxes of NH₄⁺-N, NO₃⁻-N, and TIN all showed significant
 566 seasonal variation at urban and rural sites, but not at background sites, with the
 567 highest values in summer and the lowest in winter (Fig. 7a-c).

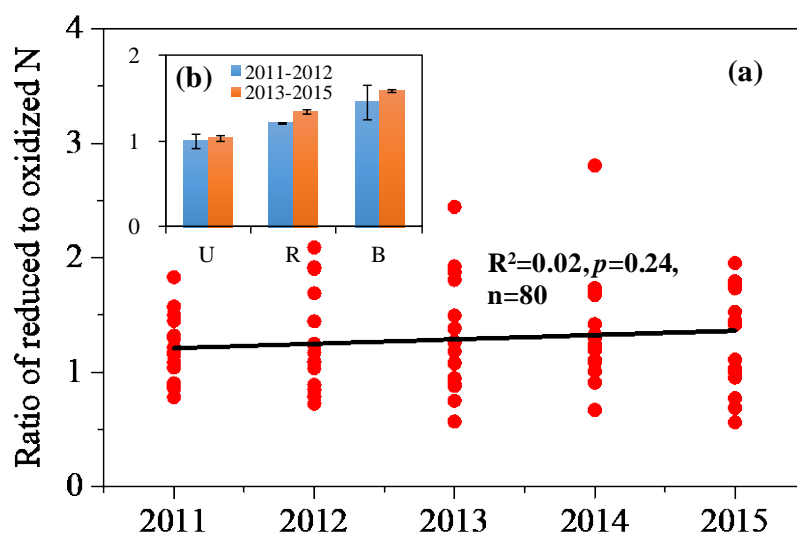


568 **Figure 7.** Seasonal mean wet/bulk deposition averaged over 2011-2015 of NH₄⁺ (a);
 569 NO₃⁻ (b) and total inorganic N (TIN): the sum of NH₄⁺ and NO₃⁻ (c) in precipitation at
 570 different land use types in eastern China and its northern and southern regions. Sp, Su,
 571 Au, and Wi represent spring, summer, autumn, and winter, respectively. U, R, and B
 572 denote urban, rural, and background sites, respectively. The number of sites for each
 573 land use type in each region can be found in Table 2. The error bars are the standard
 574 errors of means, and values without same letters on the bars denote significant
 575 differences between the seasons ($p < 0.05$).
 576

577 3.7 Spatial-temporal variability in total annual dry and wet/bulk deposition of N_r 578 species

579 In eastern China total annual mean N deposition (dry plus wet/bulk) fluxes at
 580

581 rural and background sites were comparable (on average, 44.3 ± 3.0 and 34.3 ± 0.7 kg
 582 $\text{N ha}^{-1} \text{ yr}^{-1}$, respectively), but significantly lower than those at urban sites (59.7 ± 6.1
 583 $\text{kg N ha}^{-1} \text{ yr}^{-1}$) (Tables 1 and 2, and Fig. S5, Supplement). Similar tendencies for total
 584 N deposition fluxes were observed in the southern region, while in the north a
 585 significant difference was only found between urban and background sites (Fig. S5,
 586 Supplement). From 2011 to 2015, no significant annual trend was found in the total N
 587 deposition at sixteen selected sites (Fig. S6a, Supplement). The total annual mean N
 588 deposition fluxes at three land use types showed small and non-significant reductions
 589 (1-5%) between 2011-12 and 2013-15 (Fig. S6b, Supplement). Regionally, the total
 590 fluxes at each land use type were of similar magnitude in the two periods. Also, the
 591 NH_x (wet/bulk NH_4^+ -N deposition plus dry deposition of NH_3 and particulate
 592 NH_4^+)/ NO_y (wet/bulk NO_3^- -N deposition plus dry deposition of NO_2 , HNO_3 and
 593 particulate NO_3^-) ratio showed a non-significant annual trend across all sites (Fig. 8a).
 594 At all land use types, the averaged ratios were slightly higher in the 2013-2015 period
 595 than in the 2011-2012 period (Fig. 8b).



596
 597 **Figure 8.** Annual trend of the ratio of NH_x (wet/bulk NH_4^+ -N deposition plus dry
 598 deposition of NH_3 and particulate NH_4^+) to NO_y (wet/bulk NO_3^- -N deposition plus dry
 599 deposition of NO_2 , HNO_3 and particulate NO_3^-) across sixteen selected sites (a), with
 600 a comparison between the 2011-2012 period and the 2013-2015 period for different
 601 land use types in eastern China (b). U, R, and B denote urban, rural, and background

602 sites, respectively. The number of sites with the same land use type can be found in
603 Fig. S6 in the Supplement.

604

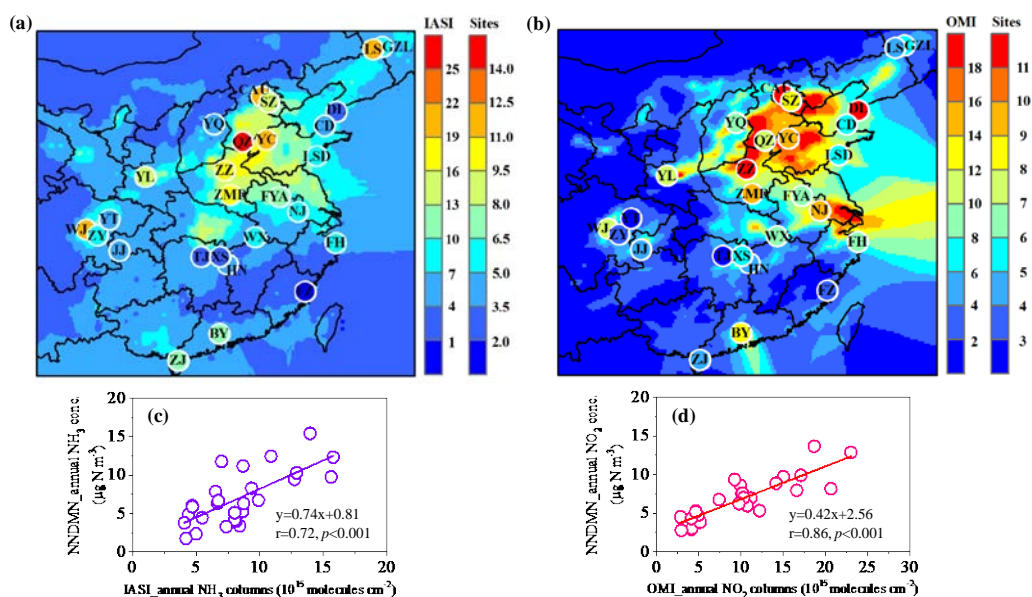
605 **4. Discussion**

606 **4.1 Comparisons of NH₃ and NO₂ measurements with satellite data**

607 Eastern China is a highly industrialized and polluted region, and has been proven
608 to be a hotspot of N_r (NH₃ and NO_x) emission and deposition globally (Vet et al., 2014;
609 Kanakidou et al., 2016). The results presented above showed that, in eastern China,
610 annual mean concentrations of measured N_r species in air and precipitation were
611 generally higher in the north than in the south (Table 1). This is likely due to higher
612 consumption of energy and application of N-fertilizers, along with lower precipitation
613 amounts in the north, previously identified as key factors affecting spatial patterns of
614 N deposition in China (Liu et al., 2013; Jia et al., 2014; Zhu et al., 2015). Because
615 only 27 sites covering a range of land use types were included in the present study,
616 additional information would be valuable in determining whether the observed spatial
617 patterns adequately represent conditions in eastern China. To address this issue, we
618 use measured NH₃ and NO₂ concentrations to evaluate remote sensing techniques for
619 retrieving NH₃ and NO₂ concentrations. If accurate, those remote sensing techniques
620 are well suited to ascertain regional species distributions. NH₃ and NO_x are primary
621 emissions with important anthropogenic emissions (Fowler et al., 2013). NO, the
622 main component of emitted NO_x, is oxidized in the atmosphere to NO₂. NO₂ is further
623 oxidized via daytime or nighttime chemistry to HNO₃ (Khoder, 2002). NH₃ and
624 HNO₃ can react to form fine particle ammonium nitrate (Seinfeld and Pandis, 2006).
625 Thus, spatial patterns of NH₃ and NO₂ observed from space can be useful indicators
626 of reduced and oxidized N_r pollution over eastern China.

627 From satellite observations (Fig. 9a, b), it can be seen that both IASI_NH₃ and
628 OMI_NO₂ columns show clearly higher values over the northern region of eastern
629 China. Overall, satellite observations and surface measurements for NH₃ and NO₂
630 (plotted on the maps of Fig. 9a, b) show a similar spatial pattern. Significant positive
631 correlations were found between IASI_NH₃ column observations and NNDMN_NH₃

632 measurements ($r=0.72$, $p<0.001$) (Fig. 9c) and between OMI_NO₂ observations and
 633 NNDMN_NO₂ measurements ($r=0.86$, $p<0.001$) (Fig. 9d) at the 27 surface
 634 measurement locations, suggesting that satellite measurements of NH₃ and NO₂ can
 635 be used to capture regional differences in NH₃ and NO₂ pollution. Looking beyond
 636 the surface measurement location, the satellite observations further confirm the
 637 existence of greater N_r pollution in the northern region of eastern China than in the
 638 southern region.



639

640 **Figure 9.** Spatial variation of atmospheric N_r in eastern China: (a)
 641 NNDMN_NH₃ concentrations vs. IASI_NH₃ columns; (b) NNDMN_NO₂
 642 concentrations vs. OMI_NO₂ columns; (c) relationship of NNDMN_NH₃
 643 concentrations vs. IASI_NH₃ columns; (d) relationship of NNDMN_NO₂
 644 concentrations vs. OMI_NO₂ columns.

645 To further explore temporal concentration variability, monthly mean satellite
 646 NH₃ and NO₂ columns are compared with monthly mean ground concentrations of
 647 NH₃ and NO₂ (Figs. S7 and S8, Supplement). The linear correlation between satellite
 648 columns and surface NH₃ concentrations is significant ($p<0.05$) at the ten sites
 649 ($r=0.32-0.87$) in the northern region and at four sites ($r=0.46-0.84$) in the southern
 650 region (Fig. S7, Supplement), while the linear correlation between satellite columns
 651 and surface NO₂ concentrations is significant at the ten sites ($r=0.28-0.68$) in the
 652 northern region and nine sites ($r=0.36-0.66$) in the southern region (Fig. S8,

653 Supplement). These results indicate that the OMI_NO₂ retrieval can well capture the
654 temporal variations of surface NO₂ concentrations over eastern China, whereas the
655 IASI_NH₃ retrievals better capture temporal variability in surface concentrations for
656 the northern region. The weak correlations observed between IASI_NH₃ observations
657 and surface measurements at ten of the fourteen sites in the southern region (Fig. S7,
658 Supplement) suggest that the IASI_NH₃ observations need to be improved for
659 investigating temporal variability in NH₃ concentration, despite that the satellite
660 observation is at a specific time of day while the surface concentrations integrate
661 across the diurnal cycle of emissions and mixing layer evolution. It should be noted
662 that a direct comparison between surface concentration and satellite column
663 measurements is inevitably affected by many factors, such as changes in boundary
664 layer height, vertical profiles of species, and interferences from cloud and aerosol
665 (Van Damme et al., 2015). Nevertheless, the ratio of satellite column to surface
666 concentration measurements is meaningful as it can provide insight into sensitivity of
667 a satellite retrieval to variation in the concentration of a gas in the surface layer (Meng
668 et al., 2008). To make a more accurate comparison, the vertical profile is
669 recommended to convert the columns to the ground concentrations in future work.

670 **4.2 Seasonal variations of N_r concentration and deposition**

671 The seasonal concentrations of N_r species in air and precipitation are dependent
672 on their sources and meteorological conditions. The highest concentrations of NH₃ in
673 summer at all land use types (Fig. 3a) are most likely due to enhanced NH₃ emission
674 from natural and fertilized soils, and biological sources such as humans, sewage
675 systems and organic waste in garbage containers (Chang et al., 2016). Zhang et al.
676 (2018) showed that NH₃ emissions in China show a strong summer peak, with
677 emissions about 50% higher in summer than spring and autumn. The lowest
678 concentrations of NH₃ in winter (Fig. 3a) can be ascribed to low NH₃ volatilization
679 under cold condition, high snow coverage, and less agricultural activities (Cao et al.,
680 2009) with large consumption of NH₃ to form NH₄NO₃ and (NH₄)₂SO₄. The lower
681 NO₂ concentration in summer (Fig. 3b) might result from higher atmospheric mixing
682 in a deeper boundary layer and a higher rate of oxidation of NO₂ to HNO₃ by reaction

683 with OH (Atkins and Lee, 1995), which is more abundant in summer due to greater
684 photochemical activity. Increased NO₂ emissions from greater coal combustion for
685 domestic heating (from middle November to middle March) in northern China may
686 also enhance NO_x emissions and subsequent NO₂ concentrations in autumn/winter
687 (Zhao et al., 2011).

688 Particulate NH₄⁺ and NO₃⁻ are mainly generated via chemical reactions between
689 NH₃ and inorganic acids (e.g., HNO₃, H₂SO₄). We found that concentrations of *p*NH₄⁺
690 and *p*NO₃⁻ at all land use types usually peaked in winter because low temperature and
691 high emissions of NO_x and SO₂ are favorable for formation of NH₄NO₃ and
692 (NH₄)₂SO₄ aerosols (Xu et al., 2016), consistent with higher concentrations of *p*NH₄⁺
693 and *p*NO₃⁻. In addition, in winter temperature inversions in combination with stable
694 meteorological conditions (e.g., low wind speed) limit horizontal and vertical
695 exchange of pollutants, and further elevated atmospheric *p*NH₄⁺ and *p*NO₃⁻ levels (Liu
696 et al., 2017). In order to identify potential transport of NO₂, *p*NH₄⁺ and *p*NO₃⁻ from
697 northern region, we calculated three-day backward trajectories arriving at five
698 southern sites (Nanjing, Baiyun, Taojing, Ziyang and Huinong) during January, April,
699 July and October using the TrajStat. The TrajStat analysis generally showed that the
700 high proportions (overall 10-36%) of air masses from the north to the south of eastern
701 China occurred in the autumn/winter, suggesting that the transport of NO₂, *p*NH₄⁺ and
702 *p*NO₃⁻ from northern China would result in increases in their respective
703 concentrations in autumn/winter south of the Qinling Mountains-Huaihe River line,
704 except at Ziyang site (Fig. S13, Supplement).

705 Nitric acid is a secondary pollutant, formed through gas phase reaction of NO₂
706 with the OH radical, reaction of NO₃ with aldehydes or hydrocarbons or hydrolysis of
707 N₂O₅ (Khoder, 2002). Nitric acid concentrations are expected to be further influenced
708 by air temperature, relative humidity and ambient NH₃ concentrations (Allen et al.,
709 1989); fine particle NH₄NO₃ formation is favored at low temperatures and high
710 relative humidities. Due to a lack of information regarding primary formation
711 pathways and influencing factors at our study sites, we cannot offer a definitive
712 explanation for small and differing seasonal patterns of HNO₃ concentrations

713 observed at the three land use types (Fig. 3c).

714 Ammonium-N and nitrate-N in precipitation mainly originate from
715 corresponding reduced (e.g., NH_3 , $p\text{NH}_4^+$) and oxidized (e.g., HNO_3 , NO_2 , $p\text{NO}_3^-$) N
716 in air, scavenged respectively, by rain and/or snow events (Seinfeld and Pandis, 2006).
717 At all land use types, the seasonal variation of NH_4^+ -N concentration in precipitation
718 was opposite to that of reduced N (the sum of NH_3 and $p\text{NH}_4^+$) concentrations (Figs.
719 4a and S9a in the Supplement), whereas a similar seasonal pattern was found between
720 NO_3^- -N and oxidized N (the sum of HNO_3 , NO_2 and $p\text{NO}_3^-$) concentrations (Figs. 4b
721 and S9b in the Supplement). Higher precipitation amounts in summer could account
722 for lower NH_4^+ -N concentrations in summer (Figs. 4a and S10 in the Supplement) due
723 to a dilution effect (Xu et al., 2015). In contrast, seasonal variations of rainwater
724 NO_3^- -N concentrations were more likely dominated by seasonal changes in oxidized
725 N concentrations rather than precipitation amount.

726 The seasonal variation of NH_3 dry deposition is generally similar to that of NH_3
727 concentration (Figs. 3a and 6a). Given comparable seasonal mean V_d for NH_3 across
728 the four seasons in most cases (Fig. S11a-c, Supplement), the seasonality of NH_3
729 deposition is mainly dominated by changes in ambient NH_3 concentrations. Seasonal
730 deposition fluxes of NO_2 and HNO_3 both differ appreciably (Fig. 6b, c), showing
731 similar variation to seasonality of their respective V_d values (Fig. S11d-i, Supplement).
732 Given weaker seasonal fluctuations of NO_2 and HNO_3 concentrations, the seasonality
733 of NO_2 and HNO_3 dry deposition are primarily functions of changes in V_d . Similar
734 analyses suggest that seasonal variation of $p\text{NO}_3^-$ dry deposition was mainly caused
735 by differences in seasonal $p\text{NO}_3^-$ concentrations (Figs. 3e and 6e), whereas that of
736 $p\text{NH}_4^+$ dry deposition was primarily driven by seasonal changes in V_d (Figs. 6c and
737 S11j-l, Supplement).

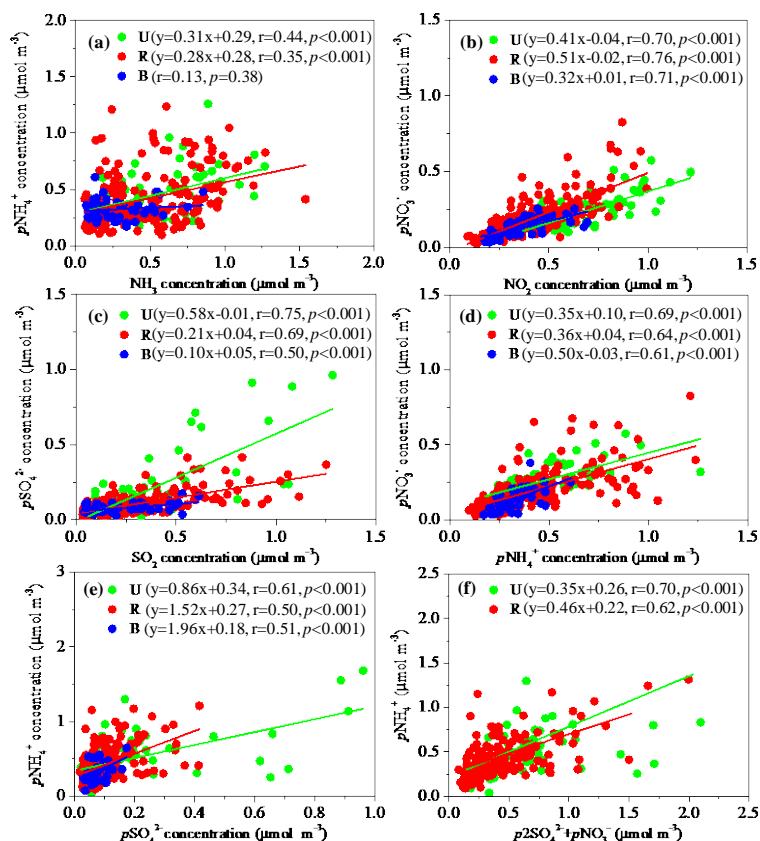
738 **4.3 The role of NH_3 in mitigation of N_r air pollution**

739 The latest pollutant emissions statistics from the Chinese Ministry of
740 Environmental Protection
741 (http://www.zhb.gov.cn/gkml/hbb/qt/201507/t20150722_307020.htm) showed that
742 total annual emissions of SO_2 and NO_x were reduced by 12.9% and 8.6% in 2014

743 (approximately 9.9 Tg S yr⁻¹ and 6.3 Tg N yr⁻¹, respectively), respectively, compared
744 with those in 2010 (approximately 11.3 Tg S yr⁻¹ and 6.9 Tg N yr⁻¹, respectively). This
745 suggests that the goal set for the 12th FYP period was fulfilled ahead of time. Our field
746 measurements demonstrate that annual mean concentrations of each N_r species and
747 total N_r did not show significant decreasing trends at most sites during the 2011-2015
748 period (Fig. S1a-f, Supplement). Furthermore, annual mean total N_r concentrations
749 showed non-significant increases (1-16%) at three land use types during the
750 2013-2015 period compared with 2011-2012 (Fig. 2f). These results together suggest
751 that N_r pollution may be not effectively mitigated in eastern China during the 12th FYP,
752 likely due to the absence of NH₃ regulations, despite enforcement of a “Zero Increase
753 Action Plan” by the Ministry of Agriculture for national fertilizer use (X. J. Liu et al.,
754 2016).

755 Ammonia is the primary alkaline gas in the atmosphere. It plays an important
756 role in formation of (NH₄)₂SO₄ and NH₄NO₃ aerosols (Seinfeld and Pandis, 2006).
757 These secondary inorganic aerosols account for 40–57 % of the PM_{2.5} concentrations
758 in eastern China (Yang et al., 2011; Huang et al., 2014). Based on monthly mean
759 molar concentrations, there were significant positive linear correlations between NH₃
760 and *p*NH₄⁺, NO₂ and *p*NO₃⁻, SO₂ and *p*SO₄²⁻, *p*NH₄⁺ and *p*NO₃⁻, and *p*NH₄⁺ and
761 *p*SO₄²⁻ at all land use land types except for a non-significant relationship of NH₃ with
762 *p*NH₄⁺ at background sites (Fig. 10a-e). These results suggest that the precursor gases
763 are responsible for the formation of secondary inorganic ions (i.e., *p*NH₄⁺, *p*NO₃⁻, and
764 *p*SO₄²⁻) locally at urban and rural sites, while secondary inorganic ions at background
765 sites likely originated from long-distance transport. The ratio of NH₃ to NH_x (NH₃
766 plus *p*NH₄⁺) concentrations at urban (0.53 ± 0.15) and rural (0.52 ± 0.16) sites
767 exceeded values at background (0.43 ± 0.16) sites. According to Walker et al. (2004),
768 a value greater than 0.5 indicates that NH_x is more likely to be from local sources as
769 opposed to long-range transport.

770



771

772 **Figure 10.** Correlations of monthly mean molar concentrations of (a) $p\text{NH}_4^+$ vs. NH_3 ;
 773 (b) $p\text{NO}_3^-$ vs. NO_2 ; (c) $p\text{SO}_4^{2-}$ vs. SO_2 ; (d) $p\text{NO}_3^-$ vs. $p\text{NH}_4^+$; (e) $p\text{NH}_4^+$ vs. $p\text{SO}_4^{2-}$; (f)
 774 $p\text{NH}_4^+$ vs. $(p2\text{SO}_4^{2-} + p\text{NO}_3^-)$ at three land use types in eastern China. The number of
 775 sites with the same land use type in each region can be found in Table 1.

776

777

778

779

780

781

782

783

784

785

786

787

It is known that NH_3 in the atmosphere is preferentially neutralized by H_2SO_4 to form $(\text{NH}_4)_2\text{SO}_4$ and/or NH_4HSO_4 , with any remainder available for potential reaction with HNO_3 to form NH_4NO_3 . At urban and rural sites, monthly mean $p\text{NH}_4^+$ concentrations significantly positively correlated with the sum of $p2\text{SO}_4^{2-}$ and $p\text{NO}_3^-$ concentrations (Fig. 10f). However, the slopes of regression equations between them were both smaller than unity (0.35 and 0.46 at urban and rural sites, respectively), indicating an incomplete neutralization of acidic species (HNO_3 and H_2SO_4) by NH_3 at urban and rural sites. In other words, NH_3 is a factor limiting the formation of secondary inorganic ions. A model simulation by Wang et al. (2011) found that, without NH_3 emission controls, NO_3^- in $\text{PM}_{2.5}$ will be enhanced by 10% in 2030 compared with 2005 in China, despite improved NO_x emissions controls. As reported by Zhang et al. (2017), total NH_3 emissions in China increased from $12.1 \text{ Tg N yr}^{-1}$ in

788 2000 to 15.6 Tg N yr⁻¹ in 2015 at an annual rate of 1.9%. In contrast, total emissions
789 of NO_x and SO₂ have decreased or stabilized in recent years, and were estimated to be
790 8.4 Tg N yr⁻¹ and 12.5 Tg S yr⁻¹ in 2014, respectively (Xia et al., 2016). Based on
791 these factors, implementation of NH₃ control strategies, together with more stringent
792 NO_x and SO₂ emission controls, should be considered to mitigate atmospheric N_r
793 pollution.

794 **4.4 The role of NH₃ emission in control of N deposition**

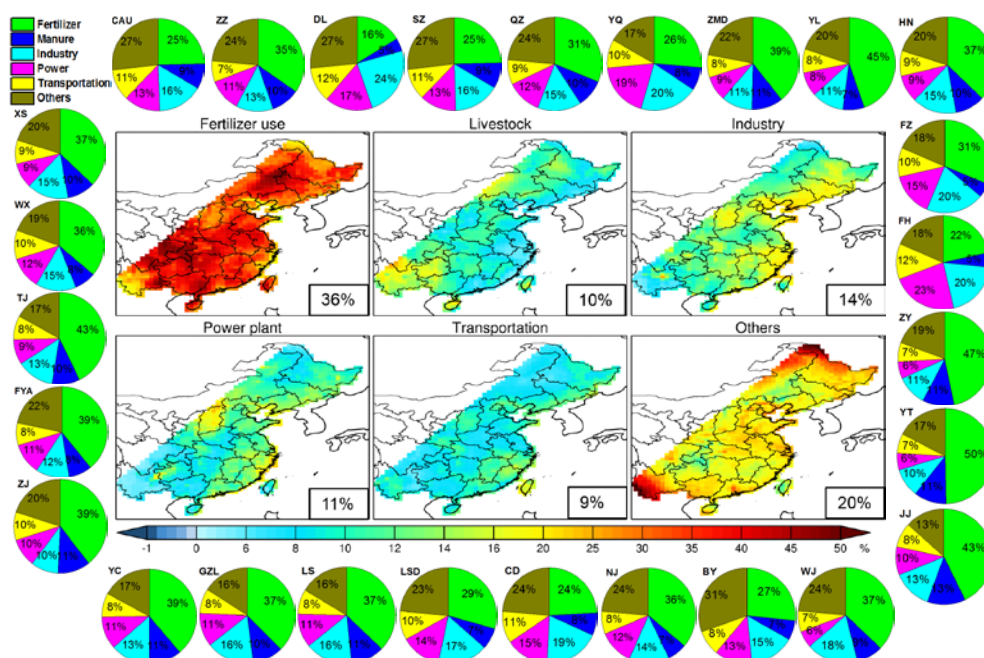
795 The present results showed that total dry N deposition fluxes at three land use
796 types were higher in the northern region of eastern China than in the southern region
797 (Table 1), mainly due to higher NH₃ dry deposition resulting from higher NH₃
798 concentrations in the north. This is especially true for northern rural sites (Table 1),
799 mostly located in the North China Plain (NCP) (see details in Xu et al. (2015)). The
800 NCP (that is, the plain areas in Beijing, Tianjin, Hebei, Henan, and Shandong
801 provinces), a highly populated region with intensive agricultural production,
802 contributes 30-40% of the total annual NH₃ emissions in China (Huang et al., 2012).
803 In addition, higher NH₃ concentration is also likely due to the higher NH₃
804 volatilization in calcareous soils than that in the acidic red soil, as mentioned in
805 Section 2.1. Total annual NH₃ emissions in northern region increased from 4.3 Tg N
806 yr⁻¹ in 2011 to 4.7 Tg N yr⁻¹ at an annual rate of 1.8%. In contrast, the emissions of
807 NO_x and SO₂ averaged 2.8 Tg N yr⁻¹ and 3.7 Tg S yr⁻¹ during 2011-2015, and
808 decreased at annual rates of 6.8 and 5.7%, respectively (details of the emissions will
809 be illustrated in Section 4.5). Such reductions may enhance free NH₃ in the
810 atmosphere. However, according to a modeling study by Han et al. (2017), the
811 influence of removing anthropogenic SO₂ emissions on dry N deposition fluxes
812 during 2010-2014 was quite weak, with the change within -0.5~0.5 (kg N ha⁻¹ yr⁻¹)
813 over most regions in China. Thus, we anticipate that reducing NH₃ emissions can
814 effectively control N deposition.

815 To further examine contributions of NH₃ emissions to total (wet plus dry) N
816 deposition at each site and over eastern China, we conducted model sensitivity tests
817 using the nested GEOS-Chem atmospheric chemistry model driven by the GEOS-5

818 assimilated meteorological fields at a horizontal resolution of $1/2^\circ \times 2/3^\circ$. The model
819 used anthropogenic emissions from the Multi-Resolution Emission Inventory of
820 China (MEIC, <http://meicmodel.org>) for the year 2010, except for NH_3 emissions that
821 are taken from the Regional Emission in Asia (REAS-v2) inventory (Kurokawa et al.,
822 2013), with an improved seasonality derived by Zhao et al. (2015). The total NH_3 and
823 NO_x emissions from each source over eastern China and its contribution to total
824 emissions in China are presented in Table S13 in the Supplement. The NH_3 and NO_x
825 emissions over eastern China are $11.6 \text{ Tg N yr}^{-1}$ and 8.5 Tg N yr^{-1} in 2010, which,
826 respectively, account for 90% and 89% of their total emissions over China.
827 Agricultural sources including fertilizer use and livestock, comprise most of the NH_3
828 emissions while fuel combustion activities, including industry, power plant, and
829 transportation contribute most of the NO_x emissions and small amounts of NH_3
830 emissions. Both NH_3 and NO_x have natural sources (including lightning, biomass
831 burning and soil emissions), but are negligible compared to anthropogenic emissions
832 over eastern China. Details of the model emissions and mechanisms have been
833 described elsewhere (Zhao et al., 2017, Xu et al., 2018).

834 We evaluate the model simulations by comparing with measured bulk (both
835 NH_4^+ -N and NO_3^- -N) fluxes. The model biases for bulk NH_4^+ -N and NO_3^- -N
836 deposition were 23 and -23%, respectively (Fig. S12, Supplement). These biases are
837 reasonable, given uncertainties in N_r emissions and predictions of meteorology. Given
838 that model evaluation is not central to this work, we presented the details in Sect. S2
839 in the Supplement. As shown in Fig. 11, fertilizer use is the dominant source of total
840 N deposition at all sites, with contributions between 16-50%. Also, over eastern China
841 the largest contribution was from fertilizer use (36%) relative to livestock (10%),
842 industry (14%), power plant (11%), transportation (9%), and other sources (20%, the
843 sum of contributions from human waste, residential activities, soil, lightning and
844 biomass burning). These results indicate that reducing NH_3 emissions by use of
845 appropriate fertilization patterns (e.g., 4 R technologies (Right amount, Right time,
846 Right form and Right application technique), Ju et al., 2009) should be a priority in
847 curbing N deposition in eastern China. This conclusion to some extent is supported by

848 increased ratios of reduced to oxidized N in the total deposition at three land use types
 849 (Fig. 8b), as the major anthropogenic source of reduced N is mainly affected by NH₃
 850 volatilized from animal excrement and the application of nitrogenous fertilizers in
 851 agriculture. Absence of NH₃ emission controls may be the main reason for a small and
 852 non-significant change in the total N deposition between 2011-12 and 2013-15 (Fig.
 853 S6, Supplement), despite enforcement of stringent emission controls on NO_x and SO₂.
 854 To test the importance of future NH₃ emission control strategies, we conducted
 855 separate model simulations which reduced NH₃ emissions from fertilizer use by 20%.
 856 The results show that a 20% reduction in fertilizer NH₃ emissions can lead to 7.4%
 857 decrease in total N deposition over Eastern China.



858
 859 **Figure 11.** Fractional contributions to total N deposition from emission sectors (i.e.
 860 fertilizer use, livestock, industry, power plant, transportation, and others including
 861 emissions from human waste, residential activities, soil, lighting and biomass burning)
 862 at the twenty-seven sites and over eastern China.

863
 864 **4.5 Deposition response to emission change**

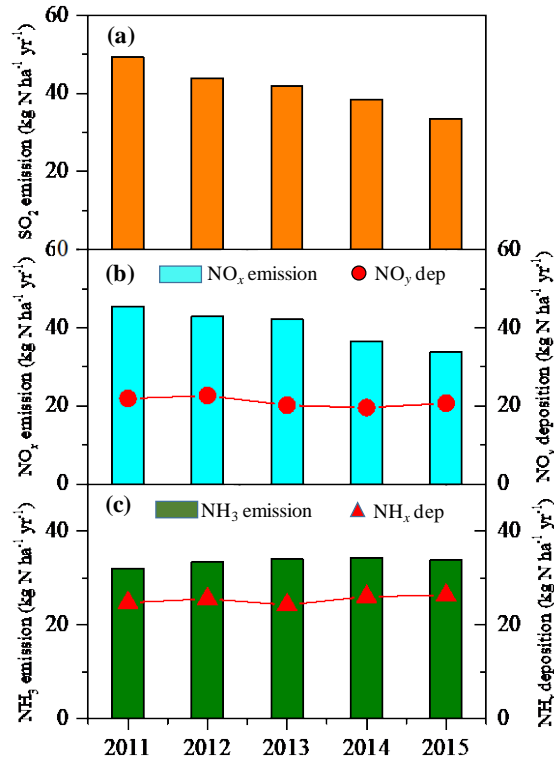
865 Similar to N_r concentrations, there were no significant decreasing trends in dry
 866 and bulk deposition of total N or of individual N_r species at almost all study sites
 867 (Figs. S3 and S4, Supplement). In addition, we found that changes in annual mean

868 deposition fluxes of various N_r species are fairly small between the 2013-2015 and
869 2011-2012 periods (Fig. 5). These results suggest that current emission controls did
870 not effectively reduce N deposition in eastern China.

871 To further assess the relationship between emission and deposition change, we
872 considered the emissions of SO_2 , NO_x and NH_3 affecting the sixteen study sites with
873 continuous and simultaneous dry and bulk deposition measurements (Fig. S6 and
874 Table S1, Supplement). The regional NH_3 emission data for 2011-2015 were derived
875 from Zhang et al. (2017), while SO_2 and NO_x emission data for 2011-2014 were
876 derived from Xia et al. (2016) (emission data for the year 2015 were provided by Prof.
877 Yu Zhao, and were unpublished). We compared these annual data with annual mean
878 deposition values from the 16 sites. It should be noted that such assessment is subject
879 to some uncertainty, as emission data was estimated based on the areas belonging to
880 eastern China.

881 A clear decreasing trend in SO_2 and NO_x emissions was observed, with
882 reductions of 32% and 25% in 2015 compared to 2011, respectively (Fig. 12a, b). This
883 reduction is directly related to the widespread use of selective catalytic reduction and
884 flue gas de-sulfurization on power plants and industries (Van der A et al., 2017), and
885 to a lesser extent to the introduction of new emission standards for cars (F. Liu et al.,
886 2016). In contrast, NH_3 emissions generally showed a gradual increasing trend
887 between 2011 and 2015 (Fig. 12c), as control strategies have not yet been enacted and
888 implemented for NH_3 emissions in China.

889



890

891 **Figure 12.** Emissions of SO₂ (a), NO_x (b) and NH₃ (c) obtained as average data from
 892 the areas belonging to eastern China, compared with deposition values in the same
 893 periods (mean values from the sixteen sites showing in Fig. S6 and Table S1 in the
 894 Supplement , 5-year averages).

895 Regarding N deposition, a non-significant increasing trend was found for NH_x
 896 (slope=0.36 kg N ha⁻¹ yr⁻¹) between the 2011 and 2015 period, whereas NO_y
 897 deposition exhibited a non-significant decreasing trend (slope=0.54 kg N ha⁻¹ yr⁻¹).
 898 Also, there were non-significant linear correlations between NH_x deposition and NH₃
 899 emission and between NO_y deposition and NO_x emission. This is not surprising given
 900 that atmospheric chemistry is complex and often behaves non-linearly (Fowler et al.,
 901 2007; Fagerli and Aas, 2008). Interactions between the different pollutants,
 902 precipitation variability, changes in the relative amounts and lifetimes of the chemical
 903 species and in gas-particle partitioning all may contribute to the lack of correlation
 904 between emission and deposition trends. Non-linearities between emission and
 905 deposition change have been described also elsewhere (Aguillaume et al., 2016;
 906 Karlsson et al., 2011). Deposition in eastern China is also influenced by emissions
 907 from outside the region, further degrading any expected correlation with local

908 emissions.

909 **4.6 Uncertainties and limitations**

910 The present study examined annual trends of concentrations of N_r species in air
911 and precipitation as well as dry and bulk N deposition based on Kendall tests and only
912 five annual data values (2011-2015). Although the test can use as few as 4 data points,
913 indications of statistically significant trends for datasets are unlikely to be truly
914 representative of the trends that are actually occurring due to in the short duration of
915 the measurement dataset. Longer time series (e.g., more than 10-year) will likely
916 allow detection of more significant time trends in future work. Another uncertainty
917 may arise from the fact that we used fixed monthly mean dry deposition velocities of
918 gaseous and particulate N_r species for the same months from June 2013 to December
919 2015. Nevertheless, the uncertainty in the V_d value did not largely affect the
920 deposition trend, as the annual trend in dry deposition of N_r species is more likely
921 driven by changes in ambient N_r concentrations than to changing deposition velocities,
922 as evident from fairly low standard deviations of annual mean V_d of N_r species at our
923 selected 27 sites between 2008 and 2012 (~ 0.029 for NH_3 , ~ 0.005 for NO_2 , ~ 0.054 for
924 HNO_3 , and ~ 0.019 for both pNH_4^+ and pNO_3^- , data were extracted from Zhao et al.
925 (2017)).

926 In addition, we did not account for inter-annual changes in meteorology, which
927 also strongly influences atmospheric N_r levels and N deposition (Xu et al., 2015,
928 2017). For example, air concentrations of NO_2 , NH_3 , and pNH_4^+ and pNO_3^- trend to
929 increase under the relatively stagnant conditions prior to a cold front's arrival and
930 decrease substantially after the cold front brings precipitation and strong winds into
931 the region (Xu et al., 2017). On the inter-annual time scale, the frequency of cold front
932 passages may be affected by large-scale circulation patterns such as the position of the
933 Siberian high for eastern China (Jia et al., 2015). For example, a large inter-annual
934 variation in precipitation amount was observed at the selected 16 sites during
935 2011-2015 (Fig. S14, Supplement), which partially lead to inter-annual changes in
936 wet/bulk N deposition. However, given that *in-situ* measurements of other
937 meteorological variables (e.g., air temperature, relative humidity, air pressure, wind

938 speed and direction) are not available, and that GEOS-5 assimilated meteorological
939 fields were updated after May 2013, an evaluation of the effect of meteorology on N_r
940 concentration and deposition is recommended for future work.

941 Uncertainties also exist in the source attribution calculated with the GEOS-Chem
942 simulations, since results largely depend on the emission inventories fed to the model.
943 Zhao et al. (2017) pointed out that uncertainties in current NH_3 emissions inventories
944 (e.g. large range of the emission value in current studies and absence of inclusion of
945 bi-directional NH_3 exchange between the land and atmosphere) may influence
946 nitrogen deposition simulation in China. Future work based on improved NH_3
947 emission inventories (e.g., Zhang et al., 2018) and including bidirectional ammonia
948 exchange with the surface is essential to better examine source attribution of N
949 deposition in China.

950 **5. Conclusion**

951 We have characterized spatial and temporal (annual and seasonal) variations in
952 concentrations and deposition of major N_r species in air (NH_3 , NO_2 , HNO_3 , pNH_4^+ ,
953 and pNO_3^-) and precipitation (NH_4^+ -N and NO_3^- -N) for three land use types (e.g.,
954 urban, rural and background) in eastern China by examining five-year (2011-2015) *in*
955 *situ* measurements at twenty-seven sites. We further examined regional features of N_r
956 pollution by comparison of satellite and surface measurements of NH_3 and NO_2 and
957 examined the sources of total N deposition over the whole region for the year 2010
958 using the GEOS-Chem model at horizontal resolution of $1/2^\circ \times 2/3^\circ$. Our major
959 results and conclusions are as follows:

960 In eastern China, annual mean concentrations and dry and bulk deposition fluxes
961 of measured N_r species in air and precipitation generally ranked in the order urban >
962 rural > background. The air concentrations and dry deposition were usually higher at
963 all land use types in the northern region of eastern China than in the southern region,
964 especially (except HNO_3) at rural sites, for which the differences reached statistically
965 significant levels. This is also true for the annual VWM concentrations of NH_4^+ -N,
966 NO_3^- -N, and TIN in precipitation, whereas bulk deposition fluxes of these species
967 were comparable for matched land use types between the northern and southern

968 regions.

969 No significant trends in the annual mean concentrations and dry and bulk
970 deposition fluxes of measured N_r species in air and precipitation were observed at
971 almost all sites during the 2011-2015 period. Also, annual averages of these values
972 showed non-significant changes between the 2011-2012 and 2013-2015 periods for all
973 land use types. Ambient total concentrations of measured N_r species showed a
974 non-significant seasonal variation at all land use types, whereas individual N_r species
975 exhibited a significant seasonal variation in most cases, except for NO_2 and pNH_4^+ at
976 urban sites, and HNO_3 at all land use types. Unlike air concentrations, dry deposition
977 of total N_r showed a consistent and significant seasonal variation for each land use
978 type, with the highest values in summer and the lowest values in winter. The V_d was a
979 dominant factor influencing seasonal variations of NO_2 , HNO_3 , and pNH_4^+
980 concentrations, while seasonal variations of NH_3 and pNO_3^- are mainly influenced by
981 their respective air concentrations. The concentrations of NH_4^+-N , $NO_3^- -N$, and TIN in
982 precipitation showed significant seasonal variations, ranking in a consistent order of
983 winter > spring > autumn ~ summer. Also, significant seasonal variations in bulk
984 deposition were also found, following in a consistent order of summer > spring ~
985 autumn > winter.

986 Both IASI satellite-retrieved NH_3 columns and OMI satellite-retrieved NO_2
987 columns over eastern China showed higher values in the north than in the south. In
988 addition, significant positive correlations were found between measured NH_3
989 concentrations and retrieved NH_3 columns, and between measured NO_2
990 concentrations and columns. These results together reveal that atmospheric N_r
991 pollution is more serious in the northern region, and also suggest that satellite
992 retrievals of NH_3 and NO_2 columns can provide useful information on spatial
993 concentration variability of these two key N_r species at a regional or national scale.
994 Weak correlations between IASI_ NH_3 observations and surface NH_3 measurements
995 were found at most selected sites, suggesting that IASI_ NH_3 observations in their
996 current state are not as readily used to accurately track temporal variability in surface
997 NH_3 concentrations.

998 Ammonia is currently not included in China's emission control policies of air
999 pollution precursors, although the necessity of mitigation has been the subject of
1000 discussion during recent years. Across all urban and rural sites, the slopes of the
1001 regression relation between $p\text{NH}_4^+$ and the sum of $p\text{SO}_4^{2-}$ and $p\text{NO}_3^-$ were both
1002 smaller than unity, indicating control of NH_3 emission not only can directly reduce
1003 ambient NH_3 concentrations, but also lower the formation of $p\text{NH}_4^+$ and $p\text{NO}_3^-$.
1004 Fertilizer use contributed 36% of the total N deposition over eastern China,
1005 suggesting reducing NH_3 emissions from fertilizer application would be an effective
1006 strategy for reducing N deposition. Overall, our findings reveal persistent serious N_r
1007 pollution during the 12th FYP period despite implementation of current emission
1008 controls, and highlight the importance of NH_3 emission control on mitigating future
1009 atmospheric N_r concentrations and deposition in eastern China.

1010

1011 **Acknowledgments**

1012 This study was supported by the National Key R&D Program of China
1013 (2017YFC0210101 & 2017YFC0210106, 2014BC954202), the National Natural
1014 Science Foundation of China (41705130, 41425007, 31421092) as well as the
1015 National Ten-thousand Talents Program of China (X.J. Liu).

1016

1017

1018

1019

1020

1021

1022

1023

1024

1025

1026

1027

1028

1029 **References**

1030 Aguiillaume, L., Rodrigo, A., and Avila, A.: Long-term effects of changing
1031 atmospheric pollution on throughfall, bulk deposition and streamwaters in a
1032 Mediterranean forest, *Sci. Total Environ.* 544, 919–928,
1033 <https://doi.org/10.1016/j.scitotenv.2015.12.017>, 2016.

1034 Allen, A. G., Harrison, R. M., and Erisman, J. W.: Field measurements of the
1035 dissociation of ammonium nitrate and ammonium chloride aerosols, *Atmos.*
1036 *Environ.*, 23, 1591–1599, 1989.

1037 Atkins, D. H. F., and Lee, D. S.: Spatial and temporal variation of rural nitrogen
1038 dioxide concentrations across the United Kingdom, *Atmos. Environ.*, 29, 223–239,
1039 1995.

1040 Bobbink, R., Hicks, K., Galloway, J., Spranger, T., Alkemade, R., Ashmore, M.,
1041 Bustamante, M., Cinderby, S., Davidson, E., and Dentener, F.: Global assessment
1042 of nitrogen deposition effects on terrestrial plant diversity: a synthesis, *Ecol. Appl.*
1043 20, 30–59, 2010.

1044 Boersma, K. F., Eskes, H. J., Veefkind, J. P., Brinksma, E. J., van der A, R. J., Sneep,
1045 M., van den Oord, G. H. J., Levelt, P. F., Stammes, P., Gleason, J. F., and Bucsela,
1046 E. J.: Near-real time retrieval of tropospheric NO₂ from OMI, *Atmos. Chem.*
1047 *Phys.*, 7, 2103–2118, <https://doi.org/10.5194/acp-7-2103-2007>, 2007.

1048 Cao, J. J., Zhang, T., Chow, J. C., Watson, J. G., Wu, F., and Li, H.: Characterization
1049 of atmospheric ammonia over Xi'an, China, *Aerosol Air Qual. Res.*, 9, 277–289,
1050 2009.

1051 Chang, Y. H., Liu, X. J., Deng, C. R., Dore, A. J., and Zhuang, G. S.: Source
1052 apportionment of atmospheric ammonia before, during, and after the 2014 APEC
1053 summit in Beijing using stable nitrogen isotope signatures, *Atmos. Chem. Phys.*, 16,
1054 11635–11647, <https://doi.org/10.5194/acp-16-11635-2016>, 2016.

1055 Dammers, E., Palm, M., Van Damme, M., Vigouroux, C., Smale, D., Conway, S.,
1056 Toon, G. C., Jones, N., Nussbaumer, E., Warneke, T., Petri, C., Clarisse, L.,
1057 Clerbaux, C., Hermans, C., Lutsch, E., Strong, K., Hannigan, J. W., Nakajima, H.,

1058 Morino, I., Herrera, B., Stremme, W., Grutter, M., Schaap, M., Wichink Kruit, R. J.,
1059 Notholt, J., Coheur, P. F., and Erisman, J. W.: An evaluation of IASI-NH₃ with
1060 ground-based Fourier transform infrared spectroscopy measurements, *Atmos.*
1061 *Chem. Phys.*, 16, 10351–10368, <https://doi.org/10.5194/acp-16-10351-2016>, 2016.

1062 Erisman, J.W., Grennfelt, P., and Sutton, M.: The European perspective on nitrogen
1063 emission and deposition. *Environ. Int.*, 29, 311–325,
1064 [https://doi.org/10.1016/S0160-4120\(02\)00162-9](https://doi.org/10.1016/S0160-4120(02)00162-9), 2003.

1065 Fagerli, H., and Aas, W.: Trends of nitrogen in air and precipitation: model results
1066 and observations at EMEP sites in Europe, 1980-2003, *Environ. Pollut.* 154,
1067 448–461, <https://doi.org/10.1016/j.envpol.2008.01.024>, 2008.

1068 Fenn, M. E., Baron, J. S., Allen, E. B., Rueth, H. M., Nydick, K. R., Geiser, L.,
1069 Bowman, W. D., Sickman, J. O., Meixner, T., Johnson, D. W., and Neitlich, P.:
1070 Ecological Effects of Nitrogen Deposition in the Western United States,
1071 *BioScience*, 53, 404–420,
1072 [https://doi.org/10.1641/0006-3568\(2003\)053\[0404:EEONDI\]2.0.CO;2](https://doi.org/10.1641/0006-3568(2003)053[0404:EEONDI]2.0.CO;2), 2003.

1073 Fowler, D., Smith, R., Muller, J., Cape, J. N., Sutton, M., Erisman, J. W., and Fagerli,
1074 H.: 2007. Long term trends in sulphur and nitrogen deposition in Europe and the
1075 cause of non-linearities, *Water Air Soil Pollut.*, 7, 41–47,
1076 <https://doi.org/10.1007/s11267-006-9102-x>, 2007.

1077 Fowler, D., Coyle, M., Skiba, U., Sutton, M. A., Cape, J. N., Reis, S., Sheppard, L. J.,
1078 Jenkins, A., Grizzetti, B., Galloway, J. N., Vitousek, P., Leach, A., Bouwman, A. F.,
1079 Butterbach-Bahl, K., Dentener, F., Stevenson, D., Amann, M., and Voss, M.: The
1080 global nitrogen cycle in the twenty-first century, *Philos. T. R. Soc. B*, 368,
1081 20130164, <https://doi.org/10.1098/rstb.2013.0164>, 2013.

1082 Fuzzi, S., Baltensperger, U., Carslaw, K., Decesari, S., van Der Gon, H. D., Facchini,
1083 M. C., Fowler, D., Koren, I., Langford, B., Lohmann, U., Nemitz, E., Pandis, S.,
1084 Riipinen, I., Rudich, Y., Schaap, M., Slowik, J. G., Spracklen, D. V., Vignati, E.,
1085 Wild, M., Williams, M., and Gilardoni, S.: Particulate matter, air quality and
1086 climate: lessons learned and future needs, *Atmos. Chem. Phys.*, 15, 8217–8299,
1087 <https://doi.org/10.5194/acp-15-8217-2015>, 2015.

1088 Galloway, J. N., Townsend, A. R., Erisman, J. W., Bekunda, M., Cai, Z., Freney, J. R.,
1089 Martinelli, L. A., Seitzinger, S. P., and Sutton, M. A.: Transformation of the
1090 Nitrogen Cycle: Recent trends, questions, and potential solutions, *Science*, 320,
1091 889–892, <https://doi.org/10.1126/science.1136674>, 2008.

1092 Ge, B. Z., Wang, Z. F., Xu, X. B., Wu, J. B., Yu, X. L., and Li, J.: Wet deposition of
1093 acidifying substances in different regions of China and the rest of East Asia:
1094 modeling with updated NAQPMS, *Environ. Pollut.*, 187, 10–21,
1095 <https://doi.org/10.1016/j.envpol.2013.12.014>, 2014.

1096 Gilbert, R. O.: *Statistical methods for environmental pollution monitoring*, John
1097 Wiley & Sons, 1987.

1098 Gruber, N. and Galloway, J. N.: An Earth-system perspective of the global nitrogen
1099 cycle, *Nature*, 451, 293–296, <https://doi.org/10.1038/nature06592>, 2008.

1100 Gu, B. J., Sutton, M. A., Chang, S. X., Ge, Y., and Jie, C.: Agricultural ammonia
1101 emissions contribute to China’s urban air pollution, *Front. Ecol. Environ.*, 12,
1102 265–266, <https://doi.org/10.1890/14.WB.007>, 2014.

1103 Guo, S., Hu, M., Zamora, M. L., Peng, J. F., Shang, D. J., Zheng, J., Du, Z. F., Wu, Z.
1104 J., Shao, M., and Zeng, L. M.: Elucidating severe urban haze formation in China,
1105 *Proc. Natl. Acad. Sci. U.S.A.*, 111, 17373,
1106 <https://doi.org/10.1073/pnas.1419604111>, 2014.

1107 Han, X., Zhang, M. G., Skorokhod, A., and Kou, X. X.: Modeling dry deposition of
1108 reactive nitrogen in China with RAMS-CMAQ, *Atmos. Environ.*, 166, 47–61,
1109 <https://doi.org/10.1016/j.atmosenv.2017.07.015>, 2017.

1110 He, N. P., Zhu, J. X., and Wang, Q. F.: Uncertainty and perspectives in studies of
1111 atmospheric nitrogen deposition in China: A response to Liu et al. (2015), *Sci.*
1112 *Total Environ.*, 520, 302–304, <https://doi.org/10.1016/j.scitotenv.2015.03.063>,
1113 2015.

1114 Huang, P., Zhang, J. B., Xin, X. L., Zhu, A. N., Zhang, C. Z., Ma, D. H., Zhu, Q. G.,
1115 Yang, S., and Wu, S. J.: Proton accumulation accelerated by heavy chemical
1116 nitrogen fertilization and its long-term impact on acidifying rate in a typical arable
1117 soil in the Huang-Huai-Hai Plain, *J. Integr. Agric.* 14, 148–157, 2015.

1118 Huang, R. J., Zhang, Y., Bozzetti, C., Ho, K. F., Cao, J. J., Han, Y., Daellenbach, K.
1119 R., Slowik, J. G., Platt, S. M., Canonaco, F., Zotter, P., Wolf, R., Pieber, S. M.,
1120 Bruns, E. A., Crippa, M., Ciarelli, G., Piazzalunga, A., Schwikowski, M.,
1121 Abbaszade, G., Schnelle-Kreis, J., Zimmermann, R., An, Z., Szidat, S.,
1122 Baltensperger, U., El Haddad, I., and Prevot, A. S.: High secondary aerosol
1123 contribution to particulate pollution during haze events in China, *Nature*, 514,
1124 218–222, <https://doi.org/10.1038/nature13774>, 2014.

1125 Huang, X., Song, Y., Li, M. M., Li, J. F., Huo, Q., Cai, X. H., Zhu, T., Hu, M., and
1126 Zhang, H. S: A high-resolution ammonia emission inventory in China, *Global*
1127 *Biogeochem. Cycles* 26, GB1030, <https://doi.org/10.1029/2011GB004161>, 2012.

1128 Ianniello, A., Spataro, F., Esposito, G., Allegrini, I., Rantica, E., Ancora, M. P., Hu,
1129 M., and Zhu, T.: Occurrence of gas phase ammonia in the area of Beijing (China),
1130 *Atmos. Chem. Phys.*, 10, 9487–9503, <https://doi.org/10.5194/acp-10-9487-2010>,
1131 2010.

1132 Jia, B., Wang, Y., Yao, Y., and Xie, Y.: A new indicator on the impact of large-scale
1133 circulation on wintertime particulate matter pollution over China, *Atmos. Chem.*
1134 *Phys.*, 15, 11919–11929, <https://doi.org/10.5194/acp-15-11919-2015>, 2015.

1135 Jia, Y. L., Yu, G. R., He, N. P., Zhan, X. Y., Fang, H. J., Sheng, W. P., Zuo, Y.,
1136 Zhang, D. Y., and Wang, Q. F.: Spatial and decadal variations in inorganic nitrogen
1137 wet deposition in China induced by human activity, *Sci. Rep.*, 4, 3763,
1138 <https://doi.org/10.1038/srep03763>, 2014.

1139 Jia, Y. L.; Yu, G. R.; Gao, Y. N.; He, N. P.; Wang, Q. F.; Jiao, C. C.; and Zuo, Y.:
1140 Global inorganic nitrogen dry deposition inferred from ground and space-based
1141 measurements, *Sci. Rep.*, 6, 19810, <https://doi.org/10.1038/srep19810>, 2016.

1142 Ju, X. T., Xing, G. X., Chen, X. P., Zhang, S. L., Zhang, L. J., Liu, X. J., Cui, Z. L.,
1143 Yin, B., Christie, P., Zhu, Z. L., and Zhang, F. S.: Reducing environmental risk by
1144 improving N management in intensive Chinese agricultural systems, *Proc. Natl.*
1145 *Acad. Sci. U. S. A.* 106, 3041-3046, <https://doi/10.1073/pnas.0902655106>, 2009.

1146 Kanakidou, M., Myriokefalitakis, S., Daskalakis, N., and Fanourgakis, G.: Past,
1147 present, and future atmospheric nitrogen deposition, *J. Atmos. Sci.*, 73,

1148 160303130433005, <https://doi.org/10.1175/JAS-D-15-0278.s1>, 2016.

1149 Karlsson, G. P., Akselsson, C., Hellsten, S., and Karlsson, P. E.: Reduced European
1150 emissions of S and N effects on air concentrations, deposition and soil water
1151 chemistry in Swedish forests, *Environ. Pollut.* 159, 3571–3582.
1152 <https://doi.org/10.1016/j.envpol.2011.08.007>, 2011.

1153 Khoder, M. I.: Atmospheric conversion of sulfur dioxide to particulate sulfate and
1154 nitrogen dioxide to particulate nitrate and gaseous nitric acid in an urban area,
1155 *Chemosphere*, 49, 675–684, 2002.

1156 Krotkov, N. A., Mclinden, C. A., Li, C., Lamsal, L. N., Celarier, E. A., Marchenko, S.
1157 V., Swartz, W. H., Bucsela, E. J., Joiner, J., Duncan, B. N., Boersma, K. F.,
1158 Veefkind, J. P., Levelt, P. F., Fioletov, V. E., Dickerson, R. R., He, H., Lu, Z. F.,
1159 and Streets, D. G.: Aura OMI observations of regional SO₂ and NO₂ pollution
1160 changes from 2005 to 2015, *Atmos. Chem. Phys.*, 16, 4605–4629,
1161 <https://doi.org/10.5194/acp-16-4605-2016>, 2016.

1162 Kurokawa, J., Ohara, T., Morikawa, T., Hanayama, S., JanssensMaenhout, G., Fukui,
1163 T., Kawashima, K., and Akimoto, H.: Emissions of air pollutants and greenhouse
1164 gases over Asian regions during 2000–2008: Regional Emission inventory in Asia
1165 (REAS) version 2, *Atmos. Chem. Phys.*, 13, 11019–11058,
1166 <https://doi.org/10.5194/acp-13-11019-2013>, 2013.

1167 Li, H., Zhang, Q., Zheng, B., Chen, C., Wu, N., Guo, H., Zhang, Y., Zheng, Y., Li, X.,
1168 and He, K.: Nitrate-driven urban haze pollution during summertime over the North
1169 China Plain, *Atmos. Chem. Phys.*, 18, 5293–5306,
1170 <https://doi.org/10.5194/acp-18-5293-2018>, 2018.

1171 Li, Y., Niu, S., and Yu, G.: Aggravated phosphorus limitation on biomass production
1172 under increasing nitrogen loading: a meta-analysis, *Global Change Biol.*, 22,
1173 934–943, <https://doi.org/10.1111/gcb.13125>, 2016.

1174 Liang, X., Zou, T., Guo, B., Li, S., Zhang, H. Z., Zhang, S. Y., Huang, H., and Chen,
1175 S. X.: Assessing Beijing's PM_{2.5} pollution: severity, weather impact, APEC and
1176 winter heating, *Proc. R. Soc. A.*, 471, 20150257,
1177 <https://doi.org/10.1098/rspa.2015.0257>, 2015.

1178 Liu, F., Beirle, S., Zhang, Q., van der A, R. J., Zheng, B., Tong, D., and He, K.: NO_x
1179 emission trends over Chinese cities estimated from OMI observations during 2005
1180 to 2015, *Atmos. Chem. Phys.*, 17, 9261–9275,
1181 <https://doi.org/10.5194/acp-17-9261-2017>, 2017.

1182 Liu, L., Zhang, X. Y., Zhang, Y., Xu, W., Liu, X. J., Zhang, X. M., Feng, J. L., Chen,
1183 X. R., Zhang, Y. H., Lu, X. H., Wang, S. Q., Zhang, W. T., and Zhao, L. M.: Dry
1184 particulate nitrate deposition in China, *Environ. Sci. Technol.*, 51, 5572,
1185 <https://doi.org/10.1021/acs.est.7b00898>, 2017a.

1186 Liu, L., Zhang, X., Xu, W., Liu, X., Li, Y., Lu, X., Zhang, Y., and Zhang, W.:
1187 Temporal characteristics of atmospheric ammonia and nitrogen dioxide over China
1188 based on emission data, satellite observations and atmospheric transport modeling
1189 since 1980, *Atmos. Chem. Phys.*, 17, 9365–9378,
1190 <https://doi.org/10.5194/acp-17-9365-2017>, 2017b.

1191 Liu, X. J., Duan, L., Mo, J. M., Du, E. Z., Shen, J. L., Lu, X. K., Zhang, Y., Zhou, X.
1192 B., He, C. E., and Zhang, F. S.: Nitrogen deposition and its ecological impact in
1193 China: An overview, *Environ. Pollut.*, 159, 2251–2264, [https://doi.org/](https://doi.org/10.1016/j.envpol.2010.08.002)
1194 [10.1016/j.envpol.2010.08.002](https://doi.org/10.1016/j.envpol.2010.08.002), 2011.

1195 Liu, X. J., Zhang, Y., Han, W. X., Tang, A., Shen, J. L., Cui, Z. L., Vitousek, P.,
1196 Erisman, J. W., Goulding, K., Christie, P., Fangmeier, A., and Zhang, F. S.:
1197 Enhanced nitrogen deposition over China, *Nature*, 494, 459–462,
1198 <https://doi.org/10.1038/nature11917>, 2013.

1199 Liu, X. J., Vitousek, P., Chang, Y. H., Zhang, W. F., Matson, P., and Zhang, F. S.:
1200 Evidence for a historic change occurring in China, *Environ. Sci. Technol.*, 50,
1201 505–506, <https://doi.org/10.1021/acs.est.5b05972>, 2016.

1202 Lu, C. Q. and Tian, H. Q.: Spatial and temporal patterns of nitrogen deposition in
1203 China: Synthesis of observational data, *J. Geophys. Res.*, 112, D22S05,
1204 <https://doi.org/10.1029/2006JD007990>, 2007.

1205 Lu, C. Q. and Tian, H. Q.: Half-century nitrogen deposition increase across China: A
1206 gridded time-series data set for regional environmental assessments, *Atmos.*
1207 *Environ.*, 97, 68–74, <https://doi.org/10.1016/j.atmosenv.2014.07.061>, 2014.

1208 Marchetto, A., Rogora, M., and Arisci, S.: Trend analysis of atmospheric deposition
1209 data: A comparison of statistical approaches, *Atmos. Environ.*, 64, 95–102, 2013.

1210 Meng, Z. Y., Xu, X. B., Wang, T., Zhang, X. Y., Yu, X. L., Wang, S. F., Lin, W. L.,
1211 Chen, Y. Z., Jiang, Y. A., and An, X. Q.: Ambient sulfur dioxide, nitrogen dioxide,
1212 and ammonia at ten background and rural sites in China during 2007–2008, *Atmos.*
1213 *Environ.*, 44, 2625–2631.

1214 Meng, Z. Y., Xu, X. B., Lin, W. L., Ge, B. Z., Xie, Y. L., Song, B., Jia, S. H., Zhang,
1215 R., Peng, W., Wang, Y., Cheng, H. B., Yang, W., and Zhao, H.: Role of ambient
1216 ammonia in particulate ammonium formation at a rural site in the North China
1217 Plain, *Atmos. Chem. Phys.*, 18, 167–184, <https://doi.org/10.5194/acp-18-167-2018>,
1218 2018.

1219 MEPC (Ministry of Environmental Protection of the People’s Republic of China):
1220 Report on Environmental Quality in China, 2010. Available online at:
1221 http://jcs.mep.gov.cn/hjzl/zkgb/2010zkgb/201106/t20110602_211579.htm, 2011.

1222 Miyazaki, K., Eskes, H., Sudo, K., Boersma, K. F., Bowman, K., and Kanaya, Y.:
1223 Decadal changes in global surface NO_x emissions from multi-constituent satellite
1224 data assimilation, *Atmos. Chem. Phys.*, 17, 807–837,
1225 <https://doi.org/10.5194/acp-17-807-2017>, 2017.

1226 Pan, Y. P., Wang, Y. S., Tang, G. Q., and Wu, D.: Wet and dry deposition of
1227 atmospheric nitrogen at ten sites in Northern China, *Atmos. Chem. Phys.*, 12,
1228 6515–6535, <https://doi.org/10.5194/acp-12-6515-2012>, 2012.

1229 Pan, Y. P., Wang, Y. S., Zhang, J. K., Liu, Z. R., Wang, L. L., Tian, S. L., Tang, G.
1230 Q., Gao, W. K., Ji, D. S., and Song, T.: Redefining the importance of nitrate during
1231 haze pollution to help optimize an emission control strategy, *Atmos. Environ.*, 141,
1232 197–202, <http://dx.doi.org/10.1016/j.atmosenv.2016.06.035>, 2016.

1233 Pinder, R. W., Walker, J. T., Bash, J. O., Cady-Pereira, K. E., Henze, D. K., Luo, M.
1234 Z., Osterman, G. B., and Shephard, M. W.: Quantifying spatial and seasonal
1235 variability in atmospheric ammonia with in situ and space-based observations,
1236 *Geophys. Res. Lett.*, 38, L04802, <https://doi.org/10.1029/2010GL046146>, 2011.

1237 Russell, A. R., Valin, L. C., and Cohen, R. C.: Trends in OMI NO₂ observations over

1238 the United States: effects of emission control technology and the economic
1239 recession, *Atmos. Chem. Phys.*, 12, 12197–12209,
1240 <https://doi.org/10.5194/acp-12-12197-2012>, 2012.

1241 Salmi, T., Maatta, A., Anttila, P., Ruoho-Airola, T., and Amnell, T.: Detecting trends
1242 of annual values of atmospheric pollutants by the Mann–Kendall test and Sen's
1243 slope estimates—the Excel template application MAKESENS. Publications on Air
1244 Quality No. 31, Finnish Meteorological Institute, Helsinki, Finland, 2002.

1245 Seinfeld, J. H. and Pandis, S. N.: Atmospheric chemistry and physics: from air
1246 pollution to climate change, 2nd Edn., Wiley Interscience, New Jersey, 2006.

1247 She, W.: Hu Huanyong: father of China's population geography, *China Popul. Today*
1248 15, 1–20, 1998.

1249 Souri, A. H., Choi, Y., Jeon, W., Woo, J.-H., Zhang, Q., and Kurokawa, J.-i.: Remote
1250 sensing evidence of decadal changes in major tropospheric ozone precursors over
1251 East Asia, *J. Geophys. Res.*, 122, 2474–2492,
1252 <https://doi.org/10.1002/2016JD025663>, 2017.

1253 Tang, Y. S., Simmons, I., van Dijk, N., Di Marco, C., Nemitz, E., Dammgén, U.,
1254 Gilke, K., Djuricic, V., Vidic, S., and Gliha, Z.: European scale application of
1255 atmospheric reactive nitrogen measurements in a low-cost approach to infer dry
1256 deposition fluxes, *Agr. Ecosyst. Environ.*, 133, 183–195, <https://doi.org/10.1016/j.agee.2009.04.027>, 2009.

1258 Theil, H.: A Rank-Invariant Method of Linear and Polynomial Regression Analysis,
1259 in: Henri Theil's Contributions to Economics and Econometrics, edited by: Raj, B.
1260 and Koerts, J., *Advanced Studies in Theoretical and Applied Econometrics*,
1261 Springer Netherlands, 345–381, 1992.

1262 Tian, S. L., Pan, Y. P., Liu, Z. R., Wen, T. X., and Wang, Y. S.: Size-resolved aerosol
1263 chemical analysis of extreme haze pollution events during early 2013 in urban
1264 Beijing, China, *J. Hazard. Mater.*, 279, 452–460, <https://doi.org/10.1016/j.jhazmat.2014.07.023>, 2014.

1266 Van Damme, M., Clarisse, L., Dammers, E., Liu, X., Nowak, J. B., Clerbaux, C.,
1267 Flechard, C. R., Galycaux, C., Xu, W., and Neuman, J. A.: Towards validation of

1268 ammonia (NH₃) measurements from the IASI satellite, *Atmos. Meas. Tech.*, 8,
1269 1575–1591, <https://doi.org/10.5194/amt-8-1575-2015>, 2015.

1270 van der A, R. J., Mijling, B., Ding, J., Koukouli, M. E., Liu, F., Li, Q., Mao, H., and
1271 Theys, N.: Cleaning up the air: effectiveness of air quality policy for SO₂ and NO_x
1272 emissions in China, *Atmos. Chem. Phys.*, 17, 1775–1789,
1273 <https://doi.org/10.5194/acp-17-1775-2017>, 2017.

1274 Vet, R., Artz, R. S., Carou, S., Shaw, M., Ro, C.-U., Aas, W., Baker, A., Bowersox, V.
1275 C., Dentener, F., Galy-Lacaux, C., Hou, A., Pienaar, J. J., Gillett, R., Forti, M. C.,
1276 Gromov, S., Hara, H., Khodzher, T., Mahowald, N. M., Nickovic, S., Rao, P. S. P.,
1277 and Reid, N. W.: A global assessment of precipitation chemistry and deposition of
1278 sulfur, nitrogen, sea salt, base cations, organic acids, acidity and pH, and
1279 phosphorus, *Atmos. Environ.*, 93, 3–100, <https://doi.org/10.1016/j.atmosenv.2013.10.060>, 2014.

1281 Walker, J. T., Whitall, D. R., Robarge, W., and Paerl, H. W.: Ambient ammonia and
1282 ammonium aerosol across a region of variable ammonia emission density, *Atmos.*
1283 *Environ.*, 38, 1235–1246, 2004.

1284 Wang, G. H., Zhang, R. Y., Gomez, M. E., Yang, L. X., Zamora, M. L., Hu, M., Lin,
1285 Y., Peng J. F., Guo, S., Meng, J. J., Li, J. J., Cheng, C. L., Hu, T. F., Ren, Y. Q.,
1286 Wang, Y. S., Gao, J., Cao, J. J., An, Z. S., Zhou, W. J., Li, G. H., Wang, J. Y., Tian,
1287 P. F., Marrero-Ortiz, W., Secret J., Du, Z. F., Zheng, J., Shang, D. J., Zeng, L. M.,
1288 Shao, M., Wang, W. G., Huang, Y., Wang, Y., Zhu, Y. J., Li, Y. X., Hu, J. X., Pan,
1289 B. W., Cai, L., Cheng, Y. T., Ji, Y. M., Zhang, F., Rosenfeld, D., Liss, P. S., Duce,
1290 R. A., Kolb, C. E., and Molina, M. J.: Persistent sulfate formation from London
1291 Fog to Chinese haze, *Proc. Natl. Acad. Sci. U.S.A.*, 113, 13630, <https://doi.org/10.1073/pnas.1616540113>, 2016.

1293 Wang, S. X., Xing, J., Jang, C. R., Zhu, Y., Fu, J. S., and Hao, J. M.: Impact
1294 assessment of ammonia emissions on inorganic aerosols in East China using
1295 response surface modeling technique, *Environ. Sci. Technol.*, 45, 9293–9300,
1296 <https://doi.org/10.1021/es2022347>, 2011.

1297 Wen, L., Chen, J. M., Yang, L. X., Wang, X. F., Xu, C. H., Sui, X., Yao, L., Zhu, Y.

1298 H., Zhang, J. M., Zhu, T., and Wang, W. X.: Enhanced formation of fine particulate
1299 nitrate at a rural site on the North China Plain in summer: The important roles of
1300 ammonia and ozone, *Atmos. Environ.*, 101, 294–302,
1301 <http://dx.doi.org/10.1016/j.atmosenv.2014.11.037>, 2015.

1302 Wesely, M. L.: Parameterization of surface resistances to gaseous dry deposition in
1303 regional-scale numerical-models, *Atmos. Environ.*, 23, 1293–1304, 1989.

1304 Whitburn, S., Van Damme, M., Clarisse, L., Bauduin, S., Heald, C. L., Hadji-Lazaro,
1305 J., Hurtmans, D., Zondlo, M. A., Clerbaux, C., and Coheur, P. F.: A flexible and
1306 robust neural network IASINH₃ retrieval algorithm, *J. Geophys. Res.-Atmos.*, 121,
1307 6581–6599, <https://doi.org/10.1002/2016JD024828>, 2016.

1308 Xia, Y. M., Zhao, Y., and Nielsen, C. P.: Benefits of China's efforts in gaseous
1309 pollutant control indicated by the bottom-up emissions and satellite observations
1310 2000–2014, *Atmos. Environ.*, 136, 43–53, [https://doi.](https://doi.org/10.1016/j.atmosenv.2016.04.013)
1311 [org/10.1016/j.atmosenv.2016.04.013](https://doi.org/10.1016/j.atmosenv.2016.04.013), 2016.

1312 Xu, W., Luo, X.S., Pan, Y.P., Zhang, L., Tang, A.H., Shen, J.L., Zhang, Y., Li, K.H.,
1313 Wu, Q.H., Yang, D.W., Zhang, Y.Y., Xue, J., Li, W.Q., Li, Q.Q., Tang, L., Lu,
1314 S.H., Liang, T., Tong, Y.A., Liu, P., Zhang, Q., Xiong, Z.Q., Shi, X.J., Wu, L.H.,
1315 Shi, W.Q., Tian, K., Zhong, X.H., Shi, K., Tang, Q.Y., Zhang, L.J., Huang, J.L., He,
1316 C.E., Kuang, F.H., Zhu, B., Liu, H., Jin, X., Xin, Y.J., Shi, X.K., Du, E.Z., Dore,
1317 A.J., Tang, S., Collett, J.L., Goulding, K., Sun, Y.X., Ren, J., Zhang, F.S., and Liu,
1318 X.J.: Quantifying atmospheric nitrogen deposition through a nationwide monitoring
1319 network across China. *Atmos. Chem. Phys.*, 15, 12345–12360, [https://doi.](https://doi.org/10.5194/acp-15-12345-2015)
1320 [org/10.5194/acp-15-12345-2015](https://doi.org/10.5194/acp-15-12345-2015), 2015.

1321 Xu, W., Wu, Q. H., Liu, X. J., Tang, A. H., Dore, A. J., and Heal, M. R.:
1322 Characteristics of ammonia, acid gases, and PM_{2.5} for three typical land-use types
1323 in the North China Plain, *Environ. Sci. Pollut. Res.*, 23, 1158–1172, [https://doi.](https://doi.org/10.1007/s11356-015-5648-3)
1324 [org/10.1007/s11356-015-5648-3](https://doi.org/10.1007/s11356-015-5648-3), 2016.

1325 Xu, W., Song, W., Zhang, Y., Liu, X., Zhang, L., Zhao, Y., Liu, D., Tang, A., Yang,
1326 D., Wang, D., Wen, Z., Pan, Y., Fowler, D., Collett Jr., J. L., Erisman, J. W.,
1327 Goulding, K., Li, Y., and Zhang, F.: Air quality improvement in a megacity:

1328 implications from 2015 Beijing Parade Blue pollution control actions, *Atmos.*
1329 *Chem. Phys.*, 17, 31–46, <https://doi.org/10.5194/acp-17-31-2017>, 2017.

1330 Xu, W., Zhao, Y. H., Liu, X. J., Dore, A. J., Zhang, L., Liu, L., and Cheng, M.:
1331 Atmospheric nitrogen deposition in the Yangtze River basin: Spatial pattern and
1332 source attribution, *Environ. Pollut.*, 232, 546–555,
1333 <https://doi.org/10.1016/j.envpol.2017.09.086>, 2018.

1334 Yang, F., Tan, J., Zhao, Q., Du, Z., He, K., Ma, Y., Duan, F., Chen, G., and Zhao, Q.:
1335 Characteristics of PM_{2.5} speciation in representative megacities and across China,
1336 *Atmos. Chem. Phys.*, 11, 5207–5219, <https://doi.org/10.5194/acp-11-5207-2011>,
1337 2011.

1338 Yang, Y. H., Li, P., He, H. L., Zhao, X., Datta, A., Ma, W. H., Zhang, Y., Liu, X. J.,
1339 Han, W. X., Wilson, M. C., and Fang, J. Y.: Long-term changes in soil pH across
1340 major forest ecosystems in China, *Geophys. Res. Lett.*, 42,
1341 <https://doi.org/10.1002/2014GL062575>, 2015.

1342 Zhao, Y., Nielsen, C. P., Lei, Y., McElroy, M. B., and Hao, J.: Quantifying the
1343 uncertainties of a bottom-up emission inventory of anthropogenic atmospheric
1344 pollutants in China, *Atmos. Chem. Phys.*, 11, 2295–2308,
1345 <https://doi.org/10.5194/acp-11-2295-2011>, 2011.

1346 Zhang, L., Chen, Y. F., Zhao, Y. H., Henze, D. K., Zhu, L. Y., Song, Y., Paulot, F.,
1347 Liu, X. J., Pan, Y. P., and Huang, B. X.: Agricultural ammonia emissions in China:
1348 reconciling bottom-up and top-down estimates, *Atmos. Chem. Phys.*, 18, 339–355,
1349 <https://doi.org/10.5194/acp-18-339-2018>, 2018.

1350 Zhang, L. M., Gong, S. L., Padro, J., and Barrie, L.: A size-segregated particle dry
1351 deposition scheme for an atmospheric aerosol module, *Atmos. Environ.*, 35,
1352 549–560, [https://doi.org/10.1016/s1352-2310\(00\)00326-5](https://doi.org/10.1016/s1352-2310(00)00326-5), 2001.

1353 Zhang, Q., Duan, F. K., He, K. B., Ma, Y. L., Li, H. Y., Kimoto, T., and Zheng, A. H.:
1354 Organic nitrogen in PM_{2.5} in Beijing, *Front. Env. Sci. Eng.*, 9, 1004–1014,
1355 <https://doi.org/10.1007/s11783-015-0799-5>, 2015.

1356 Zhang, X. M., Wu, Y. Y., Liu, X. J., Reis, S., Jin, J. X., Dragosits, U., Damme, Van
1357 M., Clarisse, L., Whitburn, S., and Coheur, P. F.: Ammonia emissions may be

1358 substantially underestimated in China, *Environ. Sci. Technol.*, 51, 12089-12096,
1359 <https://doi.org/10.1021/acs.est.7b02171>, 2017.

1360 Zhao, Y., Zhang, L., Pan, Y., Wang, Y., Paulot, F., and Henze, D. K.: Atmospheric
1361 nitrogen deposition to the northwestern Pacific: seasonal variation and source
1362 attribution, *Atmos. Chem. Phys.*, 15, 10905–10924,
1363 <https://doi.org/10.5194/acp-15-10905-2015>, 2015.

1364 Zhao, Y., Zhang, L., Chen, Y. F., Liu, X. J., Xu, W., Pan, Y. P., and Duan, L.:
1365 Atmospheric nitrogen deposition to China: a model analysis on nitrogen budget and
1366 critical load exceedance, *Atmos. Environ.*, 153, 32–40,
1367 <https://doi.org/10.1016/j.atmosenv.2017.01.018>, 2017.

1368 Zhu, J. X., He, N. P., Wang, Q. F., Yan, G. F., Wen, D., Yu, G. R., and Jia, Y. L.: The
1369 composition, spatial patterns, and influencing factors of atmospheric wet nitrogen
1370 deposition in Chinese terrestrial ecosystems, *Sci. Total Environ.*, 511, 777–785,
1371 <https://doi.org/10.1016/j.scitotenv.2014.12.038>, 2015.